ELECTRICAL RESISTIVITY AS A MEASURE OF CHANGE OF STATE IN SUBSTRATES: DESIGN, DEVELOPMENT AND VALIDATION OF A MICROPROCESSOR-BASED SYSTEM

Dong D. Le, B.S.

Thesis Prepared for the Degree of

MASTER OF SCIENCE

UNIVERSITY OF NORTH TEXAS

December 2009

APPROVED:

Vijay Vaidyanathan, Major Professor
Robert B. Hayes, Committee Member
Nandika D'Souza, Committee Member
Jaycee H. Chung, Committee Member
Elias Kougianos, Program Coordinator
Nourredine Boubekri, Chair of the Department of Engineering Technology
Michael Monticino, Dean of the Robert B. Toulouse School of Graduate Studies

Le, Dong D. Electrical resistivity as a measure of change of state in substrates: Design, development and validation of a microprocessor-based system. Master of Science (Engineering Systems), December 2009, 102 pp., 4 tables, 45 figures, 37 references

Smart structures are relevant and significant because of their relevance to phenomena such as hazard mitigation, structural health monitoring and energy saving. Electrical resistance could potentially serve as an indicator of structural well-being or damage in the structure. To this end, the development of a microprocessor-based automated resistance measurement system with customized GUI is desired.

In this research, a nodal electrical resistance acquisition circuit (NERAC) system was designed. The system hardware interfaces to a laptop, which houses a customized GUI developed using DAQFactory software. Resistance/impedance was measured using DC/AC methods with four-point probes technique, on three substrates. Baseline reading before damage was noted and compared with the resistance measured after damage. The device was calibrated and validated on three different substrates. Resistance measurements were taken from PVDF samples, composite panels and smart concrete. Results conformed to previous work done on these substrates, validating the effective working of the NERAC device.

ACKNOWLEDGEMENTS

I would like to acknowledge my major professor Prof. Vijay Vaidyanathan who encouraged, guided and helped me throughout my thesis research. Without his support, the research works for the thesis would not be possible.

I also would like to express my sincere gratitude to Dr. Jaycee Chung of Global Contour Ltd., who initially offered the research topic, guided me throughout the course of the research works, and provided financial support for the research works.

I would like to thank Prof. Robert B. Hayes and Prof. Nandika A. D'Souza for the design suggestions and guidance as thesis committee members. Especially, Prof. D'Souza was kind enough to allow me to use her material testing laboratory to perform test article resistivity measurement experiments.

There are a number of people whom I owe for their friendship and support, whose names cannot be possibly mentioned in this limited space. I deeply owe them. Also, I must say that I truly enjoyed working with Shailesh Vidhate, Ph.D. candidate in Materials Science & Engineering Dept and thank for his helping me to operate the MTS machine.

Most importantly, the research work would not be possible without my family's support, my loving wife, Jenny Le and two beautiful children Newton and Preston Le whom I love dearly.

TABLE OF CONTENTS

Page

LIST OF TABLES

LIST OF FIGURES

CHAPTER 1

INTRODUCTION AND REVIEW OF LITERATURE

Carbon fiber composites are inherently piezoresistive and thus, damage self-sensing is possible as a smart material [1]. Self-sensing means structural composite material works as a sensor. Recent research work performed by Chung et al. [28-37] under a National Science Foundation grant has proven its validity for potential damage and strain self-sensing. Smart structures are relevant and significant because of their relevance to phenomena such as hazard mitigation, structural health monitoring and energy saving. Cement-based materials that exhibit piezoresistivity with sufficient magnitude contain electrically conductive fibers. This allows materials to sense their own strain and damage [2, 3]. Smart structures have the ability to sense certain stimuli and respond appropriately. A structural composite, which is itself a sensor, is said to be self-sensing [4]. In this class of materials are several cement-matrix and polymer matrix materials. For example, a new class of engineered cementitious composites (ECC) has been developed that use a low volume fraction of short carbon fibers as mentioned above. This class of materials changes its electrical properties in response to damage [5]. Smart concrete is an innovation in itself – a concrete that can sense strain or stress. The sensing ability is induced by the use of admixtures (carbon fibers). Smart concrete exhibits the property of piezoresistivity. This refers to the change in resistivity with strain, not to be confused with piezoelectricity.

1.1. Problem Statements

Using embedded devices such as optical fibers one can monitor damage in structural material composites. However, the embedded technique has some drawbacks – high cost of sensors and equipment, poor durability of the sensor, limited functional volume and degradation of mechanical properties of the material due to embedding of the sensor.

1.2. Research Approach

Given these drawbacks, the use of self-sensing materials to monitor strain and damage, assumes significance. The self-sensing ability of a composite material such as the carbon fiber polymer matrix can be shown through the measurement of the electrical resistance/resistivity of the system [6]. Thus, there is a need for the development of simple, reproducible methods using compact, state-of-the-art electronics that would facilitate the measurement of resistance for self-sensing of composite materials. Electrical resistance or resistivity could potentially serve as an indicator of damage in materials. McCarter et al. [7] have shown the effectiveness monitoring of concrete structures to determine concrete resistivity. Basheer et al. demonstrated the use of resistance/resistivity to determine the extent of chlorine ion penetration in concrete. This is significant because chlorine ion penetration results in the deterioration of concrete due to cracking and spalling [8].

Electrical resistance/resistivity could serve as an indicator of damage in materials. If a voltage potential, *V,* is applied across a composite material, electricity will flow

parallel to the applied field with current, *I*, proportional to the applied voltage potential [9]. Ohm's Law relates the resistance of the material, R, to the current and voltage: $V = IR$. Since the resistance of the material is dependent upon the geometry of the specimen, resistance is normalized by the specimen geometry and is reported as a measure of a material's resistivity, ρ. Assuming the voltage potential is applied to a specimen by rectangular plates of area, *A*, which are separated by length, *L*, the material resistivity is defined as follows [9]:

$$\rho = R\,A / L \qquad (1)$$

The resistivity of cement and concrete materials can vary widely depending on various factors. In general, their resistivity can span from 1×10^4 to 1×10^8 Ω-cm [5]; in this range, cement-based materials are considered to be semiconductors. In contrast, metals are highly conductive materials with resistivities below 1×10^{-4} Ω-cm while insulators, like paraffin, have resistivities above 1×10^8 Ω-cm [5].

1.3. Methods of Measurement

Measuring methods can be classified as either direct current (DC) or alternating current (AC) resistance test methods. In DC resistance tests, a constant voltage potential is applied to generate electrical current in a composite specimen. Two common Kelvin techniques for determining the resistivity of a semiconductor material are the four-point collinear probe method, and the two-point probe technique. The most common way of

measuring the resistivity of a semiconductor material is using a four-point collinear probe [10]. This technique involves bringing four equally spaced probes in contact with a material of unknown resistance. As shown in Figure 2, the two outer probes are used for sourcing current and the two inner probes are used for measuring the resulting voltage drop across the surface of the sample. In the case of the two-point probe technique, let consider the material in the shape of a rectangular bar of length *l*, height *h*, and width *w*. Copper wires are attached to both ends of the bar [10]. A voltage source applies a voltage *V* across the bar, causing a current *I* to flow through the bar. (Alternatively, a current source could force current through the sample bar, while a voltmeter in parallel with the current source measures the voltage induced across the sample bar.) The amount of current *I* that flows through the bar is measured by the ammeter, which is connected in series with the bar and voltage source. The voltage drop across the ammeter should be negligible. Ohm's law gives the resistance R of the bar:

$$R = V / I \qquad (2)$$

R = Resistance in ohms, *V* = Voltage in volts and *I* = Current in amps

The physical dimensions can be measured with a ruler, a micrometer, or other appropriate instrument. This method is comparatively easy to use and works well when proper electrode contacts are used. The two-point resistivity of the material is then given by:

$$\rho = (R\ w\ h) / l \qquad (3)$$

Where ρ is the resistivity in Ohm-m, *R* is the measured resistance in Ohms, and *w*- width, *h* - height, and *l*- length are the measured physical dimensions of the sample bar in meters.

1.4. Previous Research

Previous work by D.D.L. Chung et al. has demonstrated that for piezoresistivity-based strain sensing using carbon fiber-reinforced cement (152 mm [6 in.] specimens under compression) in the elastic regime. The four-point-probe method of electrical resistance measurement was found to be more effective than the two-probe method in that it provides gauge factor (fractional change in resistance per unit strain) that is higher and that varies less with the strain amplitude [3]. The two-probe method was shown to suffer from the resistance increasing irreversibly in the first few loading cycles due to minor degradation of the electrical contacts.

Previous research of graduate student, they have demonstrated feasibility of using nodal resistance as a measure of detecting damage in composite substrates [11] using four-point probe technique. Our results have shown that electrical resistance could potentially yield information about damage inflicted on a composite material [11]. In addition to demonstrating proof of concept for a compact, easy to use nodal resistance measurement system controlled by a computer, the research clearly showed that there was a significant difference (statistical confidence level of 95%) between resistance measurements from the composite substrate, before and after the infliction of damage.

1.5. Purposes of Research

The purposes of this research are: 1) Design and develop a low cost and higher efficiency and accuracy nodal electrical resistance acquisition circuitry (NERAC) system which consists of embedded hardware and post-processing analytical tools (software) to detect damage and strain in multifunctional materials (e.g., carbon fiber composite structure, carbon fiber mixed cement concrete, etc.). 2) Using the NERAC system to verify previous works and compare with other available instruments such as HP multimeter. To achieve those purposes, the following tasks below have to be completed

1. Use HP multimeter to measure resistances of smart concrete samples and fiber specimens using load damage.
2. Design and develop a NERAC Instrument using embedded device and electronics devices.
3. Design a graphic user interface (GUI) using DAQFactory development software tool to interface between a computer (desktop or laptop) and NERAC instrument.
4. Use NERAC system to measure resistance/resistivity of smart concrete sample and fiber specimen using load damage.
5. Compare results from 1 and 4
6. Verify results with previous works
7. Validate NERAC system

1.6. Thesis Overview

This thesis consists of six chapters. Chapter 2 discusses methods that are used to detect material damage. The third chapter emphasizes on the NERAC instrument that is developed for measuring material's resistance/resistivity. Chapter 3 has two sections: hardware and software. Chapter 4 talks about NERAC user interface tool (NUIT) which is developed by using DAQFactory development tool. Chapter 5 analyzes, compares, and verifies measuring results from previous works with results measured by using NERAC system. In addition, this chapter validates the developed NERAC system base on those analysis results. Chapter 6 summarizes the thesis research works and recommend for future update on the NERAC system.

CHAPTER 2

RESISTANCE/RESISTIVITY MEASURING METHODS

For a simply configured example of a composite panel, four electrodes will be located on the composite panel as shown in Figure 1. Electrical resistance measurement will be performed by measuring voltage through any chosen pairs of the electrodes (four-point probes technique) among them while running electrical current through another pair of electrodes. In other words, resistance is measured from the selected pairs of electrodes.

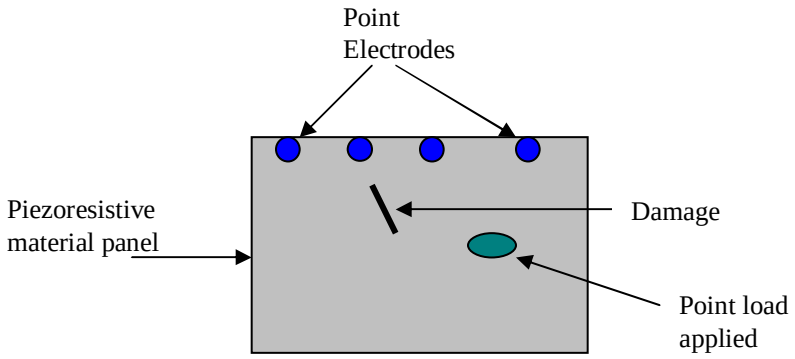

Figure 1: Diagrammatic representation of a piezoresistive concrete (smart concrete) slab showing potential position of electrodes for resistance measurement.

2.1 Resistance Measuring Techniques

There are two techniques that can be used to measure resistance. Those are two point probes and four point probes in which the four-point probes technique is firmly

used in this study. By using 4-point probes, four equally spaced probes are placed in contact with the substrate of interest; the two outer probes are used for sourcing current; and the two inner probes are used for measuring the resulting voltage drop across the surface of the sample. In general, while the two-point probe technique is simpler and easier to implement, the four-point probe technique has been proven to be more accurate. A diagram of the four-point probes technique is shown in Figure 2.

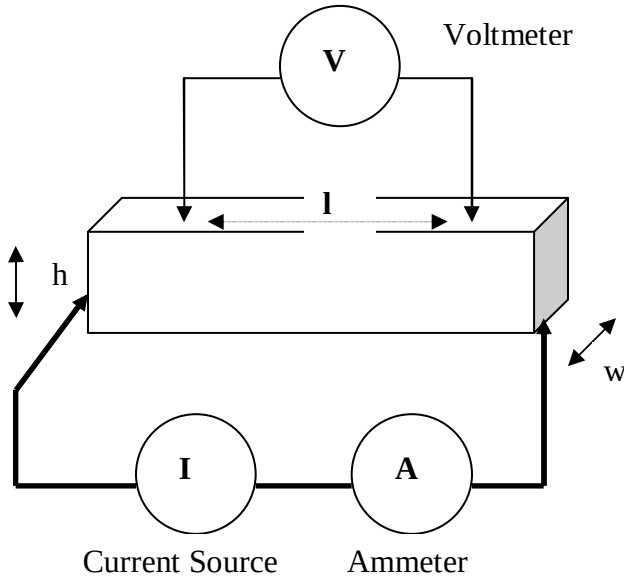

Figure 2: Probe configuration in 4-point probes technique.

The resistivity measured using this technique is expressed as:

$$\rho = (V\ w\ h)\ /I\ l \qquad (4)$$

Where,

ρ = resistivity measured in Ohm-meter

V = voltage measured by the voltmeter in Volts

w = width of the sample (m)

h = height of the sample (m)

I = current measured by the ammeter (A)

l = distance between the two points where the voltmeter makes contact

2.2 Resistance Measuring Methods

As mentioned in chapter 1, the way to measure electrical resistance of a material is applying electrical current on a material then measure the voltage drop on that material. Its resistance is calculated using equation (2). There are two type of electrical current: AC and DC in which AC is more accurate when measure resistance of a complex structure composite.

2.2.1 DC Method

DC resistance of a sample is measured using the four-point probes technique interfaced to the NERAC Instrument. In addition, the resistance from the sample is also measured using a digital multi-meter (HP 1100). The intention of the digital multi-meter is ensuring the accuracy of the NERAC unit by maintaining a standardized frame of reference. A built-in automatic pole switch is used to depolarize the object structure during measurement.

The direct current (DC) test method is the simplest technique to measure resistance in a composite sample. Unfortunately, composite materials cannot be viewed as simply being resistive; rather, the material is somewhat capacitive with charge build-up probable [5]. Referred to as the polarization effect, the DC measurement of electrical resistance is technically difficult due to an exponential rise in the measured resistance. One way to nullify the polarization effect of DC electrical resistance measurements is recording the change in resistance due to polarization for an unloaded specimen. Another approach is applying a DC voltage potential well ahead of loading the material so as to allow the resistance to plateau off due to complete polarization. However, this method is not practical for use in the field [5].

2.2.2 AC Method

An alternative method of applying voltage signals to composite materials is employing alternating current (AC) signals with equal magnitudes of positive and negative peaks. Although polarization can still be observed in AC signals, its effect can be narrowed to an acceptable range by increasing the applied AC frequency. Unlike the DC testing, the AC impedance test has little or no polarization influencing in the conductivity measurement, thus resulting in strain measurements with greater accuracy. A frequency generator circuit allowed the frequency to be adjusted between 10 Hz to 1 MHz.

Under AC condition, the impedance Z consists of the resistance R_s (real part of Z) and the reactance X_s (imaginary part of Z), i.e., $Z = R_s + jX_s$, where the subscript s refers

to a configuration in which the sample is in series connection with the measuring circuit.

AC provides both resistance and reactance information and AC is relevant to data acquisition by wireless methods. It has been found that in carbon fiber (short) reinforced mortar at 7 days of curing; the reactance Xs is a more sensitive indicator than the resistance Rs, as the fractional change in reactance exceeds the fractional change in resistance upon deformation [12]. The effect of strain on the reactance relates to the effect of strain on the polarization i.e., the direct piezoelectric effect [13], which is to be different from the piezoresistive effect.

2.3 Material Resistance

Experimental techniques implement will involve measurement of surface resistance as well as volume resistance using the four-point probes technique.

2.3.1 Surface Resistance

A composite specimen that is subjected to a load induces tension on one side and compression on the other side. To measure the surface resistance on a side of the specimen, electrical contacts is placed on the surface using the four-probe method of resistance measurement. These contacts allow for only the measurement of resistance on the side that they are placed. The experiment will use contacts on both sides of the specimen (tension and compression), so that the damaged caused to both sides of the specimen could be tracked simultaneously. The usefulness of this setup is in the fact that when flexural loading and unloading at increasing stress amplitudes, the observer can see

both the irreversible and reversible effects. The irreversible effects are due to damage and the reversible effects are due to strain [4].

2.3.2 Volume Resistance

Electrical contacts, which are on the surface but around the whole cross section of the specimen, rather than surface contacts, were used to determine the volume resistance of smart concrete specimen (bricks). The four contacts are applied to four planes that were perpendicular to the direction of the resistance measurements. This setup could potentially monitor the damage after different levels of flexural loading. The measuring of the volume resistance will be done after each level of flexural loading.

CHAPTER 3

NERAC INSTRUMENT

Nodal electrical resistance acquisition circuit (NERAC) instrument is developed using advance technology devices and components to measure resistance/resistivity of materials. The designed ideology is creating a standalone instrument that equipped with AC and DC constant current source with AC frequency varies from 10Hz to 1MHz to works as a multifunctional digital meter. Hence, NERAC device is capable to measures AC and DC currents, voltages resistances and AC frequency. Figures 3 and 4 show a completed NERAC system including a NERAC instrument connected to a computer, with pre-installed Microsoft Windows operating system and NERAC user interfacing tool (NUIT will be introduced in chapter 4).

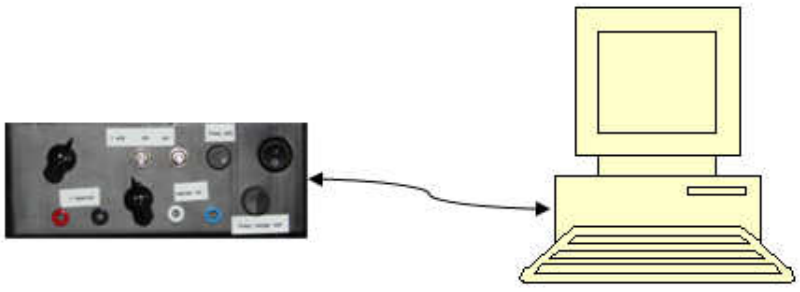

Figure 3: NERAC system.

NERAC instrument development processes comprise three main sections: electronic devices and circuits, printed circuit board (PCB), and embedded programming. The first two sections are NERAC hardware and the third one is NERAC software. Each section consists of several subsections. This chapter introduces function of every subsection and the design's details are explained in Appendix A and B.

3.1 NERAC Hardware

NERAC hardware is a compact circuit board enclosed in a small 8x6x3" enclosure for easy carrying and interfacing to a laptop or desktop computer. The designed unit has the following features: digital circuits – 8051 microcontroller, with online joint test action group (JTAG) programming capability; analog circuits – for acquisition and signal conditioning; and communication capability with a laptop or desktop computer. Figure 5 shows detail functional block diagrams of a NERAC's hardware.

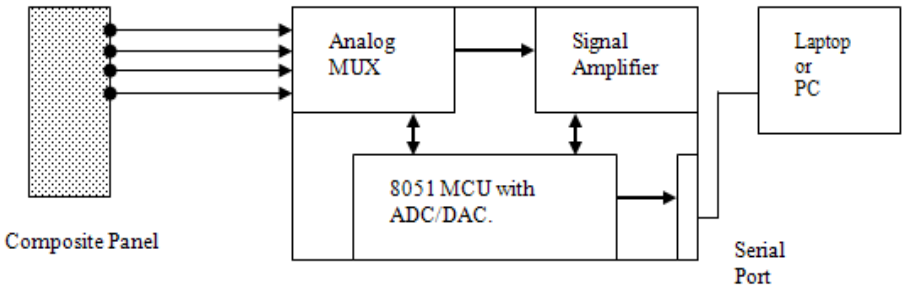

Figure 4: NERAC system's blocks diagram.

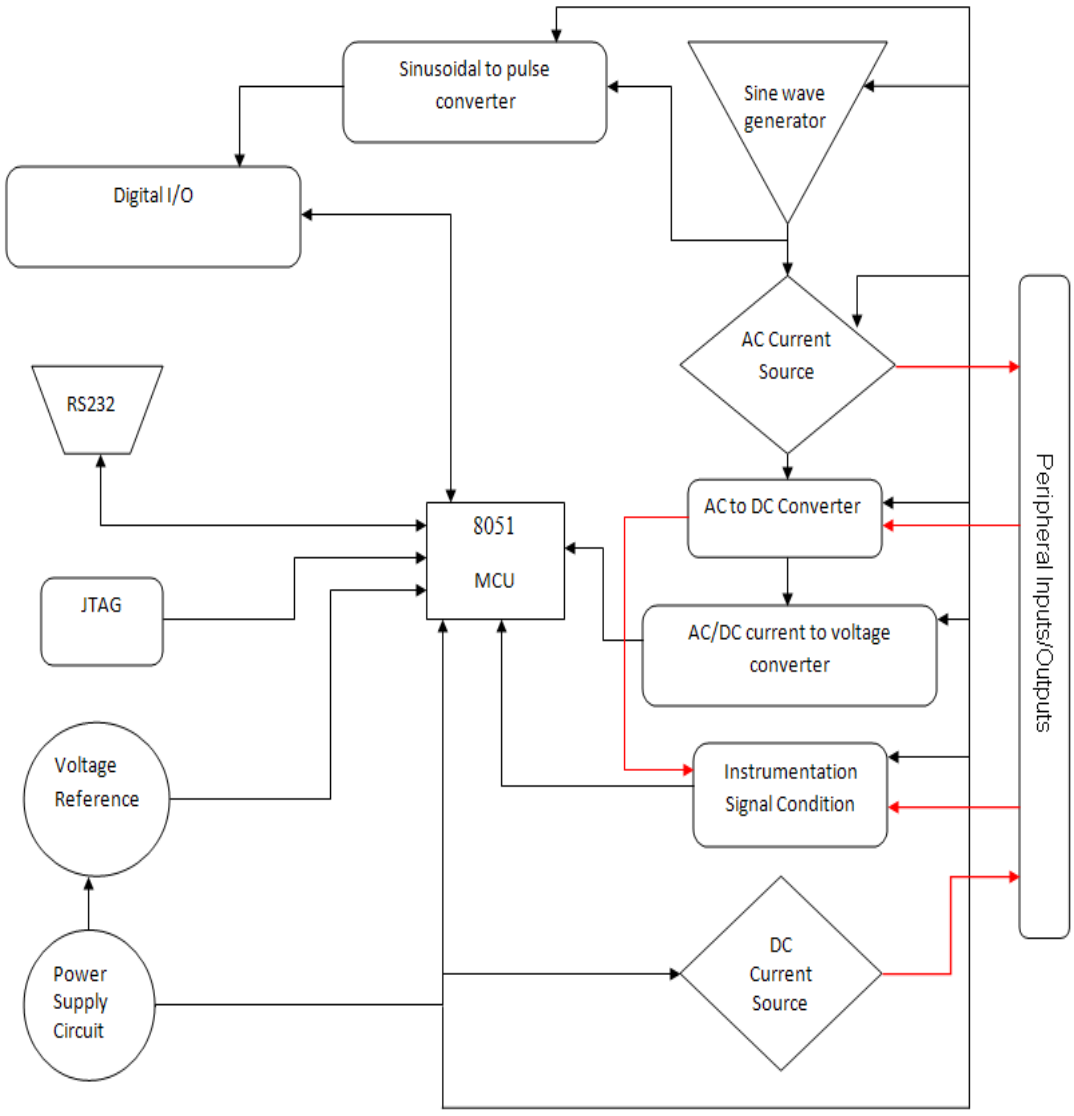

Figure 5: NERAC Instrument with detail functional blocks diagram.

3.1.1. Digital Circuits

NERAC's digital circuits consist of:

- A C8081F040 microcontroller (circuit connection in appendix A2 Figure A4
- Digital I/Os

- Serial RS 232 (UART) (circuit connection in appendix A4 Figure A6)
- JTAG (circuit connection in appendix A3 Figure A5)

3.1.1.1. C8051F040 Microcontroller

NERAC's instrument with a heart is one of the 8051 family microcontrollers manufactured by Silabs Inc, the C8051F040, which serves the function of controlling data input, processing and sending the output information to a computer. This processor is integrated with several devices to create a multi functional microcontroller unit (MCU) and can be programmed using Assembly or C language via an on-board JTAG programming.

The C8051F040 MCU has a built in two analog to digital converters (ADC), four precise analog inputs with multiplexer and multi digital I/Os with crossbar selections. It has five timers, and can operate at 25MHz clock speed for fast processing. With 64Kbyte internal memory, this MCU can store plenty of source codes, in which the NERAC application uses only 40% of that capacity. Appendix A2, Figure A4 shows the pin connection of this MCU. Appendix B1 presents a completed data short of this MCU.

3.1.1.2. Digital I/Os

C8051F040 MCU can serve up to 64 digital I/Os with crossbar enable. This crossbar capability allows designer(s) to configure each I/O to fit for a particular application. For example, the designer can reserve all digital I/O ports for digital inputs/outputs or use partial of them for other application such as in the NERAC

instrument, I use eight I/Os from port 1 for timers and UART. If an I/O is used for digital input, it has to connect with a buffer circuit to prevent damage to the MCU. For example, ‘sinusoidal to pulse converter’ is a buffer circuit between the ‘sine wave generator’ and port 3.5 of the MCU.

3.1.1.3. Serial communication

Universal asynchronous receiver/transmitter (UART) serial port (RS232) is the linkage between the MCU and a computer. It transmits data to the computer via Tx pin and receives data from the computer at Rx pin using 8 bits serial signal. The MCU’s UART device, however, has weak signals and therefore requires a signal conditioning circuitry to function as a driver or receiver for the microcontroller to be able to send and receive data properly. Appendix A4 Figure A6 shows a circuit’s construction of a MAX3223 RS-232 multichannel lines driver/receiver. This interfacing circuit boosts up signals from the MCU’s port P0.0 and P4.0 then sends them to a computer’s serial port in transmit mode. In receiver mode, this circuit amplifies signals from pin 2 and 8 of a computer’s serial port before send them to the MCU. This circuit also acts as a buffer to protect the Microcontroller from over current charge from a computer’s serial port.

3.1.1.4. Joint Test Action Group (JTAG)

JTAG connection is the microcontroller build in device to provide on chip programming function. With this JTAG, the MCU is easier to be programmed, flashed, and debugged using a compact debug adaptor.

3.1.2 Analog Circuits

NERAC instrument comprises many high efficiency electrical components with elegant design analog circuits that will delivery best functional effectiveness and low energy usage to system and they are:

- Power supply circuits with regulated outputs and coupling and filtering capacitors (appendix A1 and figure A1, figure A2 and figure A3)
- DC current source (appendix A7 and figure A9)
- AC current source
    - Sine wave generator (appendix A8.1 and figure A10)
    - Signal amplifier and voltage control current source (appendix A8.2 and figure A11)
- AC to DC converter (appendix A9 and figure A12)
- AC/DC current measurement (appendix A12 and figure A16)
- Instrumentation signal condition (appendix A10 and figure A14)
- Sine wave to pulse converter (appendix A11 and figure A15)
- Voltage references (appendix A5 and figure A7)

3.1.2.1. Power Supply Circuitries

Power supply circuits distribute multiple different regulated DC voltage levels such as 15V, -15V, and 3.3 to the system, and these voltages are filtered by decoupling capacitors to assure pure and quality power. Power supply includes internal section and external section, in which external section serves as voltage supply, and internal section serve as regulators and filters.

External section is a 15VDC voltage source, which is not part of NERAC's design, and it can be either an AC adaptor or a battery set. The external supply voltage should have a current carrier up to 1.5 Amp and output voltage tolerance of 10% to be usable.

Internal section consists of a regulated 3.3V source that divided into 3 ways: 3.3VDD, 3.3VA, and 3.3VD2 by using filter circuits, and a positive to negative voltage inverter that invert a 15VDC to -15VDC. The regulated 3.3V is a stepped down voltage from the 15VDC source by using a LM2575 chip from National Semiconductor. 3.3VDD and 3.3VD2 serve as microcontroller's power sources and 3.3VA supply voltage for other applications (described in Appendix A). In addition, parallel decoupling capacitors circuits are connected along with those 3.3V to assure analog and digital supply voltages to the microcontroller are clean and pure. SI7661 is an unregulated positive to negative voltage inverter, but its output level is an inversion of input: "Output = - Input". Therefore, if input is regulated voltage, output is also regulated voltage.

3.1.2.2. DC Current Source

The ideal of constant DC current source is that its electrical supply current to a load will not change while load resistance is changing, and this current only change when the controlled resistor is varied. It is very important to keep electrical current stay constant because electrical current is fluctuating during a measurement process will affect its output results. The current NERAC instrument can supply constant DC current to

sample with a range from 5mA to 70mA. Moreover, this range can be modified to increase up to 5A depend on application.

3.1.2.3. AC Current Source

AC current source supplies constant AC current to a sample for AC resistance/resistivity measurement. Its circuitry is more complicated than DC circuit but it provides more accurate measuring results than DC (as mentioned in Chapter 2). One of the significant parameters beside electrical current of an AC circuit is its frequency. Frequency of an AC current will affect the results of measurements conducted on samples that have reactant factor involves. Also, as mentioned in Chapter 2, higher frequency can narrow the effect of polarization, thus, AC resistance measurement not only requires constant current source but also constant frequency. NERAC's power supply is DC, hence, in order to create a constant AC current source, I have to build a sine wave generator first to create AC signal from DC supply then amplify this AC signal using an amplifying circuit and lastly, regulate its current using voltage control current source circuit.

3.1.2.3.1. Sine Wave Generator

Sine wave generator is built using a XR-2206 chip from Exar Corporation that shown in Figure A10. This circuit creates a sinusoidal signal with frequency can be varied from 10Hz to 1,000,000Hz and peak to peak amplitude oscillates symmetrically over 0V. Figure 6 shows a sample of a sinusoidal signal output with Vp-p = 5.406V and

frequency at 131.2 KHz. Vp-p is a maximum positive to negative of a sine wave's amplitude and Vp = Vp-p/2 = 2.5203V. The sinusoidal signal oscillates symmetrically over 0V; hence, maximum positive and negative amplitude of the sinusoidal is 2.5203V and -2.5203V respectively.

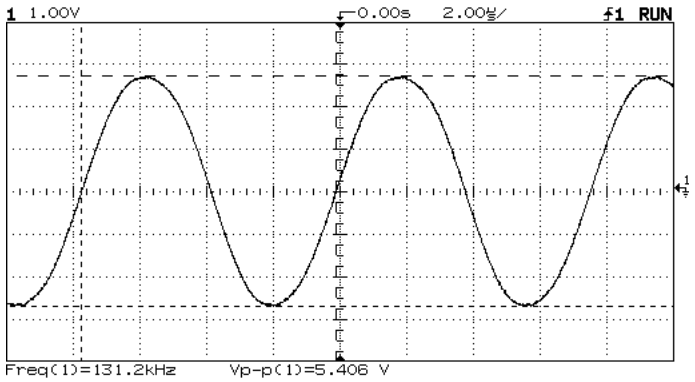

Figure 6: Sinusoidal signal.

3.1.2.3.2. AC Signal amplifier and Voltage Control Current Source (VCCS)

Power output from the sine wave generator is weak and its current is not regulated. Therefore, the AC signal amplifier will amplify the sinusoidal current before feeding to a VCCS circuit to regulate this sinusoidal current. The current output from a VCCS in Figure A11 has no ground parameter and thus, giving no electrical polarization to sample. Supply current connects to a measuring sample at High side and Low side of a VCCS op amp; current flows through that sample depends on input's voltage and resistant but not output resistant. As a result, supply current always stays constant when sample resistant change.

3.1.2.4. AC to DC converter

The microcontroller of this NERAC instrument can be programmed to take AC voltage input via HDVA, but there is only one HDVA and the NERAC's application requires at least two AC voltage inputs. Furthermore, HVDA working concurrently with other analog DC inputs requires complicated programming structure that will take more MCU's resources and consequently, slowing down the MCU's operating speed. Therefore, an easy way for the MCU to read AC signals without slowing down it processing speed is converting AC signal into corresponding DC level using RMS to DC converter circuit. Circuit in Figure A12 converts AC voltage into DC voltage. The DC output of this circuit represents the true RMS level of an AC input.

3.1.2.5. AC/DC Currents Measurement

In order for the MCU to read current from a current source, current has to be converted into DC form before input to MCU's analog input channel. This DC voltage will be calculated by multiplying with a variable, which is determined in a calibrating process, to result a corresponding current value. Converting DC current to voltage is one-step but from AC current to voltage requires two steps. Figure A16 bottom section presents a DC current to voltage converter circuit. Electrical current from a DC current source passes through a shunt resistor to load and then ground. A current sense chip measure voltage drop across that shunt resistor and output that voltage to an analog input of the MCU. The top section of Figure A16 is an AC current to voltage converter circuit. AC current is converted into DC current and this DC current is measured using a current

sense chip. Next, that DC current multiplies a calibrated variable to get the true RMS AC current. Calibrated variable is acquired from NERAC's calibration process using precise AC current meter.

3.1.2.6. Instrumentational Signal Conditioning

As described in Chapter 1, the technique of measuring resistance of a sample using 4-point probes is applying current to sample using two outer probes and measure voltage drop on that sample using two inner probes. Voltage drop between two inner probes is the voltage difference between those two probes. There are several ways to measure the potential difference between 2-point probes, and the easy but efficient method that I use in the NERAC instrument is employing instrumentation device. Figure A14 presents two simple circuits using instrumentation AD622 devices.

3.1.2.7. Sine Wave to Pulse Converter (for frequency measurement)

In AC measurement, frequency parameter also effects output resistance and that is the higher frequency, the lower resistance. Therefore, knowing the exact frequency of an AC current supply is considerable. There are many ways to measure frequency such as using frequency to voltage converter or measure a sine wave period to get frequency. The method to measure frequency that is implemented in the NERAC instrument is counting the frequency pulses for a period of 1 second then the numbers of pulse counted equal to frequency. The MCU digital input is not sufficient to take raw sinusoidal signal: first, this signal has negative voltage involve, and second, its duty cycle is not long enough for the

MCU to pick up at high frequency. Therefore, a sine wave to pulse converter is necessary to situate the problems. The MCU starts a timer and increases count by one whenever the pulse signal is HIGH and stop the timer after one second. The result of “counts” is equal to frequency.

3.1.2.8. Voltage references

There are two voltage references in the NERAC instrument: 2.4V is provided by the MCU and 3.0V comes from a voltage reference circuit. Voltage reference is required for MCU’s analog to digital converter. The NERAC instrument is designed to allow user(s) using either 2.4V or 3.0V. The 3.0V reference allows wider MCU’s analog input range. If an analog signal sends to any AIN input pin of the MCU is greater than the reference voltage, the output will only show at the reference voltage. The MCU can handle input signal higher than reference voltage, but not higher than 3.3V, without damage itself.

3.2. PCB Circuit Board

NERAC’s PCB layout is designed using PCB123™ software tool from Sunstone Circuits. PCB123™ is an all in one software tool for circuit designers. It comes with circuit schematic tool and PCB layout tool. This software allows user(s) switching and converting from one to another at any instant. It comes with hundreds of design’s features and available parts from several manufactures such as Analog Devices and Texas

Instruments to provide easy and convenience usage. Appendix B.5 presents more detail about this software.

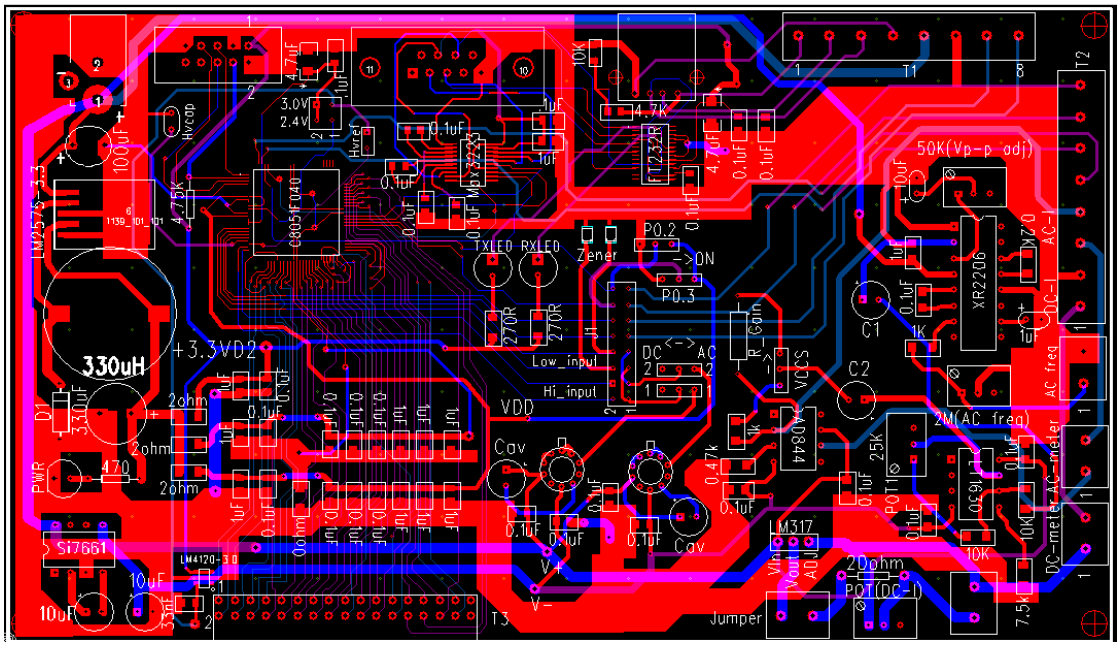

Figure 7: NERAC's PCB layout using PCB123™ software tool to design.

NERAC's PCB Circuit board is a 7"x4" board with four layers using 1oz copper and 0.062" material thickness. Most of layout footprints are using surface mount or small through holes components in order to create a small size circuit board. NERAC's layout board satisfies all the requirements of product applications such as current and frequency handling. All copper traces have a minimum of 150% handling capability to assure all the electrical parameters operate faultlessly. For example, output current of the LM2575 is 1A maximum, so the copper trace width must be 0.781mm based on the PCB trace width calculation. The trace width for the LM2575 output in the NERAC's layout is 1.5mm,

which is equal to 192%. Figure 7 presents the NERAC PCB layout and Figure 8 is a complete NERAC's circuit board

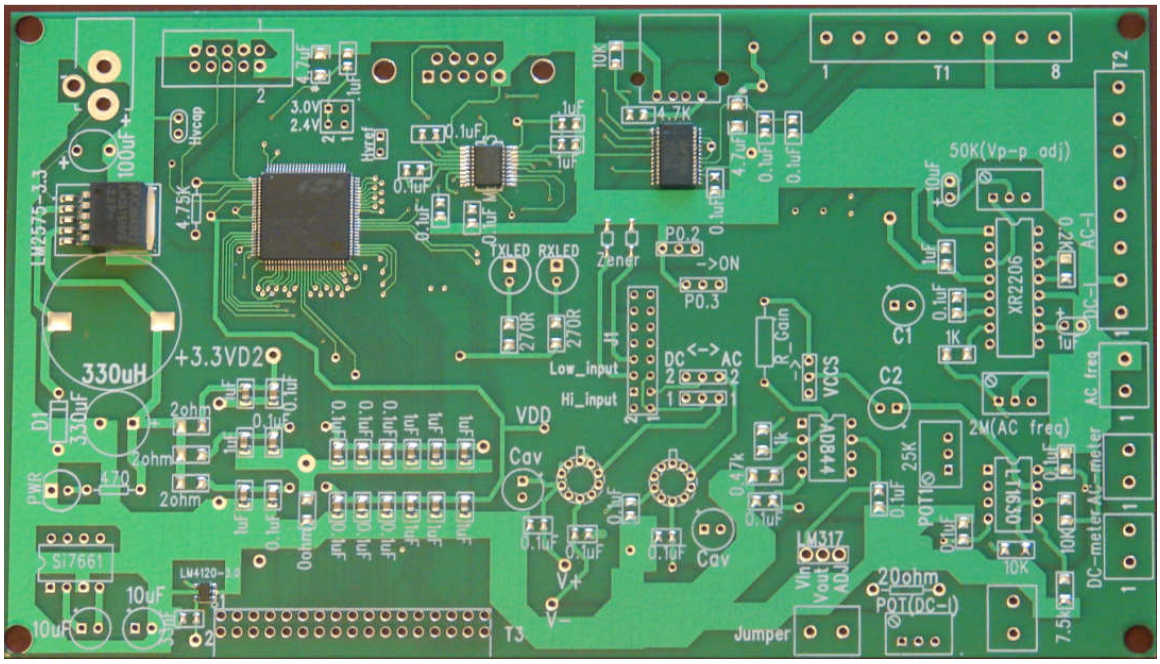

Figure 8: Completed NERAC's PCB circuit board.

3.3. Embedded Programming

The programming language that is used for the C8051F040 in the NERAC instrument is C language. The Silicon Laboratory IDE development tool with integrated Keil C51 compiler is used for codes development and debugging. Figure 9 presents a partial of the development tool windows and C codes. More details on Silicon Laboratory IDE and Keil C51 tool are in appendixes B.2 and B.3 respectively.

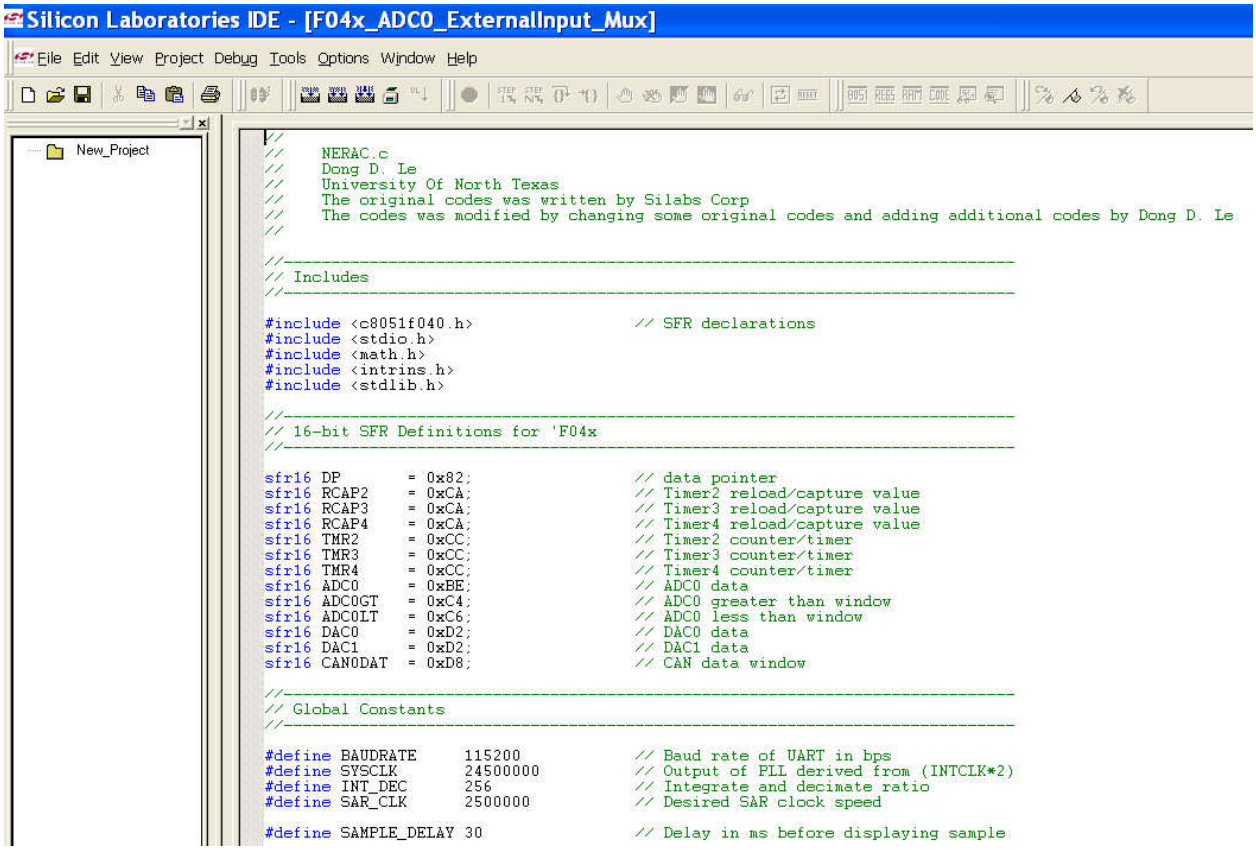

Figure 9: Silicon Laboratory IDE development tool.

The programming source codes for the NERAC instrument are originally comes from an example that provided by Silicon Laboratories, Inc when a Silicon Lab IDE software is installed into a computer. I modified these original codes by adding more codes and editing some original codes in order to make the MCU works with the NERAC's application. The NERAC codes functional flow chart shows in Figure 10 and its completed programming C codes are in appendix B4.

The main function will initialize all function calls: Oscillator_Init(), Port_Init(), UART_Init(), Timer2_Init(), Timer4_Init(), and ADC0_Init() once the program starts up.

- Oscillator_Init() function sets clock frequency for the system.

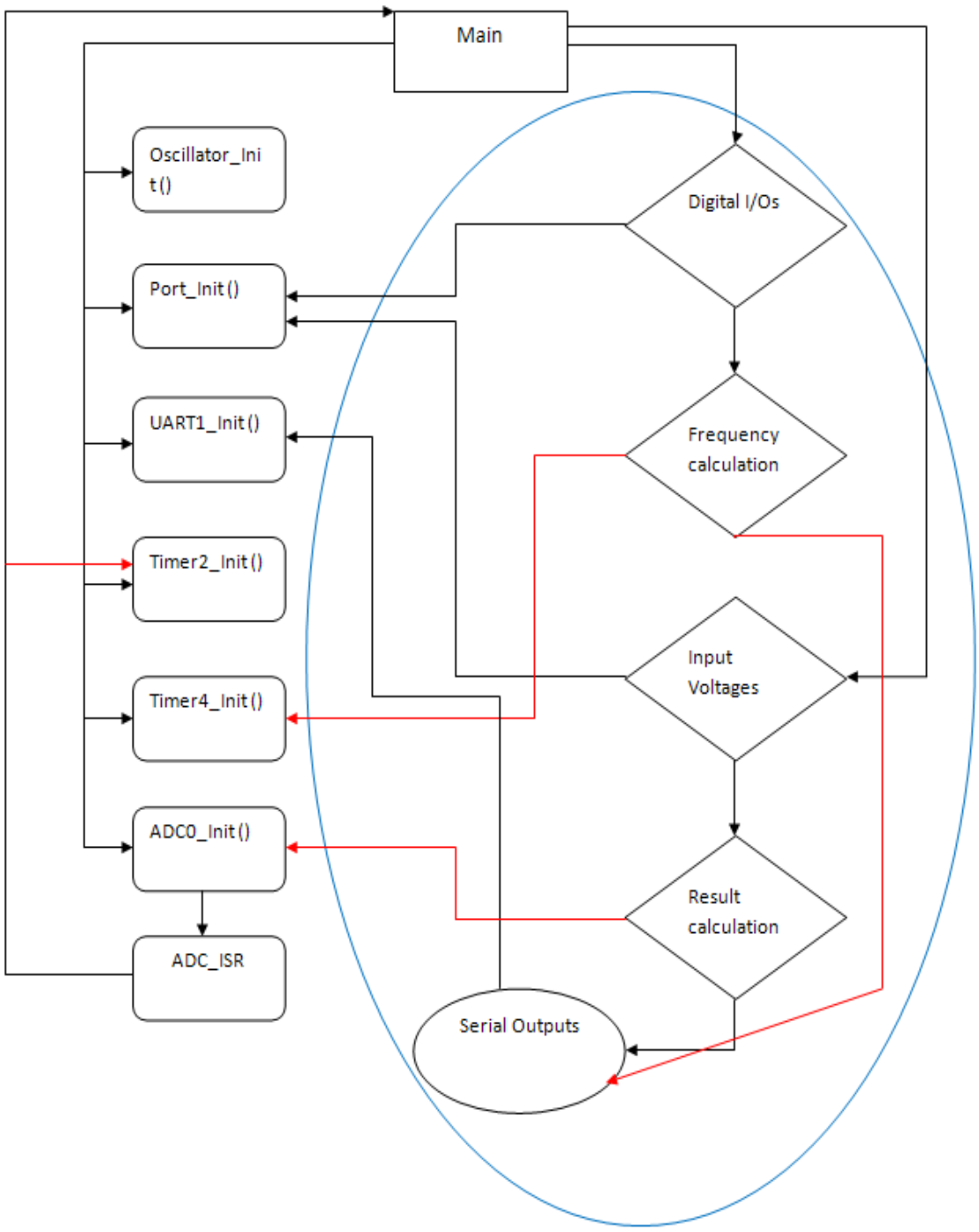

Figure 10: MCU's structural programming flow chart diagram.

- Port_Init() function selects and sets analog input ports.
- Timer2_Init() function sets timer for ADC converter. This function is called whenever ADC0_ISR() run.
- Timer4_Init() function sets timer for frequency calculation.
- ADC0_Init() function initializes ADC0 then call ADC0_Init() function after finish converting.

After main function initialized all those functions above, it then starts taking input from or output to peripherals. The left branch of the Main function in Figure 10 is a loop that continuously running until the MCU power is cut off. Inside this loop are command lines. Each command line before executed, have to call a function that associates with it. For example, digital I/Os command line calls Port_Init() function to acquire data from a digital input port then passes that data to frequency calculation. Frequency calculation calls Timer4_init() to start timer4 and stop in the next second. The numbers of pulses counted during that second equal frequency. This frequency will be sent to output and displayed on a computer screen. Next, the main function continues with input voltage command. The input voltage command line calls Port_Init() function in order to get data from analog input ports then passes the collected data to Result Calculation command. This command will call the ADC0_Init() function to do the ADC converting and send the results to serial output command. Serial output command have to call UART_Init() function in order to be able to transmit data to computer serial port. These processes are continuously looping with a delay of 30 ms.

CHAPTER 4

NERAC USER INTERFACING TOOL

NERAC user interfacing tool (NUIT) is developed by using Daqfactory development tool from Azeotech, Inc. This NUIT is designed to provide convenient functions and user-friendly interface with clear instructions page included in the software. Figure 11 presents a NUIT page with all essential electrical parameters are updating in real time (more NUIT pages are in appendix A17, A18, A19 and A20).

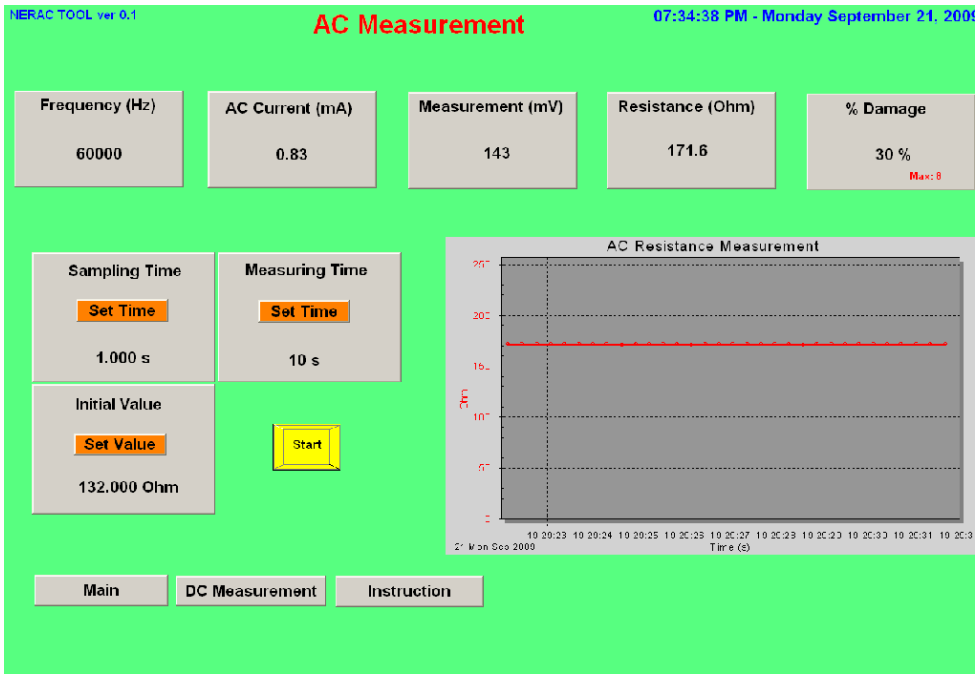

Figure 11: NERAC user interfacing tool (AC measurement page).

The developing concept of this NUIT is creating a standalone software tool that carries multiple features to provide convenient and easy usage. The NUIT features include onsite instructions, electrical parameters display, data processing, logging, and graphing. NERAC user interfacing tool allows user(s) to go to any interfacing page while or while not conducting a measurement. Also, it works as a smart tool that will not allow user(s) to perform more than one process at a time to prevent data confusion.

Figure 12 presents an operating flow chart of this software. The NUIT starts up its main page with an introduction about the software tool and explains software user's agreements and licenses that require anyone about to utilize this software tool to agree with those agreements. By clicking "Next", NUIT turns to instruction page, which contains clear instructions about how to use this program together with NERAC device. From Instruction page, one can selects to go back to main page, calibration page, AC measurement page, or DC measurement page.

- Calibration process is achieved on every finished NERAC unit, and calibrated numbers are provided with the released NERAC unit. Every time a NUIT is installed/copied to a new hard drive, it requires user(s) to resubmit the calibrated numbers into calibration page. NERAC's calibration should be performed whenever its expiration date sticker expired, and it should be calibrated with precise and reliable instruments. User(s) can choose to run AC or DC calibration by clicking on a labeled button then follow provides instructions to finish calibrating procedure.

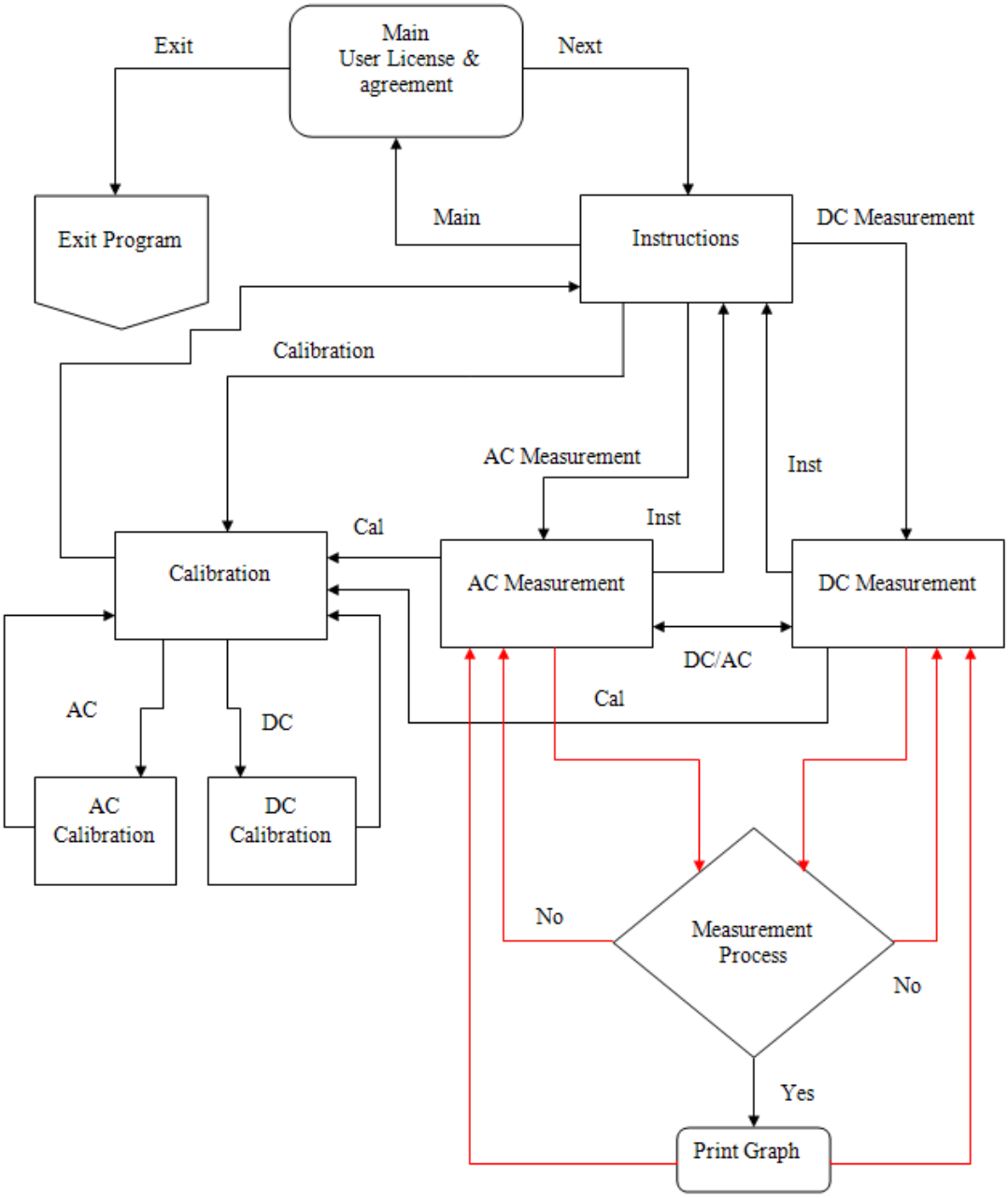

Figure 12: NUIT's operating flow chart.

- AC measurement page presents AC parameters includes frequency, AC current, measuring voltage, resistance, percentage damage, and a graph of resistance vs.

time. It only shows all of those parameters when all probes are tied to an electrical sampling load; otherwise, just frequency and current are available. Once all probes are set up and NERAC instrument is ready for an AC resistant measurement, if “Start” button is pressed, NUIT will automatically logging measured data and plotting the graph until measuring time end or stopped by user(s). Once data logging is finished, a message pop up to let user(s) select if he/she wants to save that data graph. From this page, user(s) can select to go back to instruction page or DC measurement page.

- DC measurement page show all DC parameter includes DC current, measuring voltage, resistance, percentage damage, and a graph of resistance vs. time, and not all of those parameters are available if all probes are not yet connected with sample. DC resistant measuring procedure is the same as performing an AC resistant measurement, and only one measuring process can be conducted at a time.

NUIT is an advance software tool that can save user(s) time and works. It automatically processes and calculates measured data from a NERAC Instrument then store data in a specified computer folder in real time and plot a graph after a measurement finishes. Therefore, the combination of a NERAC instrument, a personal computer with Windows OS and NUIT would create a unique standalone NERAC System that does not require any additional hardware or software to detect damage on smart composite structures.

CHAPTER 5

NERAC SYSTEM VALIDATION

5.1. System Validation

After a developed NERAC system is accomplished, the last most important process that must be done successfully is validating it. NERAC system validating procedures include:

1. Calibrating NERAC system by using it to measure low tolerance resistors (Figure 13) and then adjust the system's multiplicative variables to get output results matching with those resistor values.

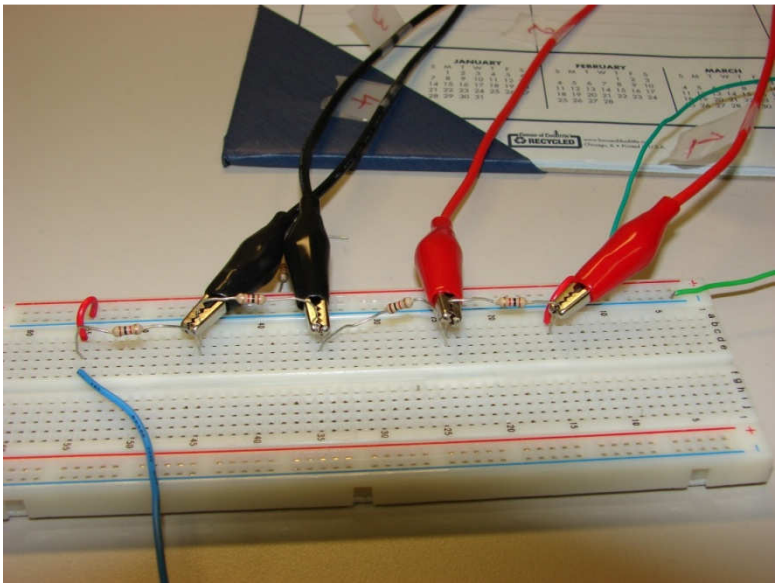

Figure 13: Calibrating NERAC System with resistors.

2. Measure an unknown sample's resistance using NERAC system
3. Measure the same unknown sample's resistance in step 2 using a precise instrument such as a HP 1100 multimeter
4. Compare results from 2 and 3

5.1.1. Calibration

Calibration is the first step to validate NERAC system and this step requires calibrator(s) follow the instructions from NUIT software properly. I calibrated the NERAC system using 0.1% tolerance resistors along with a HP 1100 digital multimeter. I performed DC calibration first and then continued with the AC. I repeated the same calibration process 3 times on 3 different resistor values to assure all calibrated values were the same.

5.1.2. Validation

Validation involves using the calibrated NERAC system along with a digital multimeter to measure resistance of an unknown resistor (step 2 and 3). The result outcomes from these two measuring instruments will be analyzed using a statistical analysis software tool (step 4). If the analyzed results are falling within 95% confident interval, the NERAC system is validated. Axial loading effects and damage effects are two types of effects that I was using during the performing material resistant measurements.

5.1.2.1. Axial loading effects

A piezoresistive nanocomposite was prepared by melt blending multiwall carbon nanotubes (MWCNT) into polyvinylidene fluoride (PVDF) [14]. The standard material test system (MTS) was used to monotonically load the PVDF sample in axial tension to initiate strain-hardening behavior [14]. Similar tests were performed using the smart concrete samples (Figure 14). The compression tests were performed on MTS 810 material test system, a universal testing machine, in which the upper plate was fixed and the bottom plate was mobile. The compression test was performed at a cycling frequency of 1/60 Hz (period = 1 minute) with loading weight of 600 lbs.

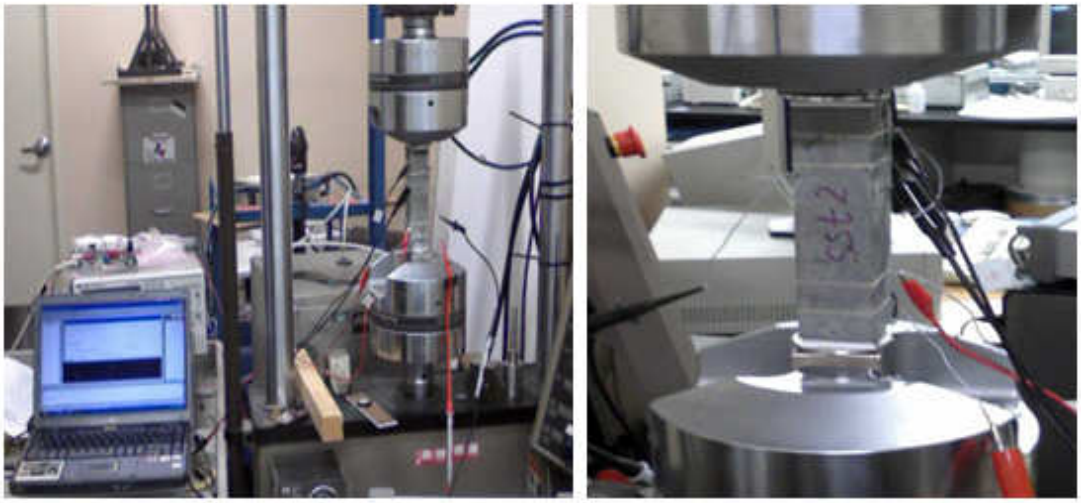

Figure 14: Smart concrete resistant measurement using MTS axial loading effect.

The axial compressive force and the displacement data were automatically recorded in a computer by the NUIT software. The data acquisition system controlling the MTS system recorded the applied load and the corresponding elongation of the plate.

The NERAC unit measured the resistances of the specimen during loading. Also along with the NERAC system, a standard digital multi-meter (HP 1100) was used to simultaneously record the resistance of the specimens. The strain was measured using a strain gage (Omega SG/KFG series) that is coupled to the composite panel. The strain gage was part of a standard Wheatstone bridge circuit whose output was connected to a data acquisition board for continuous monitoring on a computer.

5.1.2.2.Damage effects

Composite panels from helicopter blades were used in this study. Damage to the composite panel was introduced by drilling holes in the sample at various places (Figure 15). Resistance was measured with the NERAC using DC measurement method. Resistance of the panel before and after damage was compared.

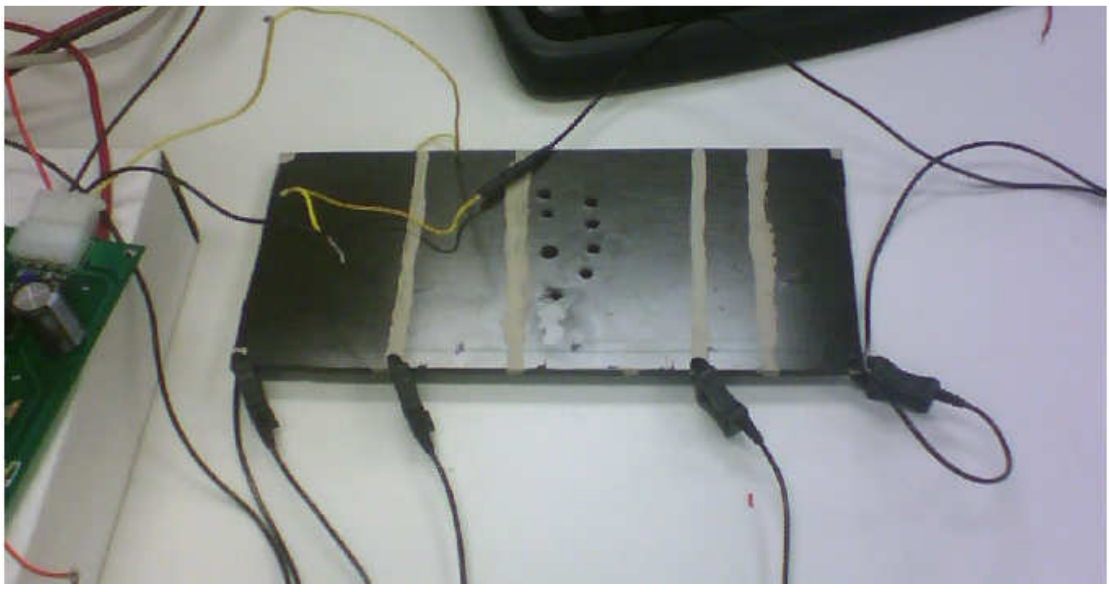

Figure 15: Damage effects on a composite panel.

5.2. Results and Discussions

5.2.1. NERAC System Calibration

Standard resistances measured using the NERAC unit was compared to those measured using a frame of reference, a HP digital multimeter. The percentage error was found to be less than 5%. Statistical analysis was performed to compare the resistance measurements made using NERAC unit to that of the resistance measured using an HP 1100 digital multimeter. This was accomplished by performing, a 'paired t-test' [15] at a significance level of 0.05. The statistical analysis was done by using Microsoft® Excel application and the differences were found to be statistically insignificant.

5.2.2. NERAC System Validation

5.2.2.1. Axial Loading Effects

An increase in resistance with an increase in pressure is called positive pressure coefficient (PPC) and a decrease in resistance with an increase in pressure is called negative pressure coefficient (NPC). Experimental results showed that at 10 wt.% of MWCNT loading in PVDF compressive stress both PPC and NPC phenomena was observed. Resistance was measured before loading (R0) and also during loading (R). In the composite system, MWCNT can be treated as incompressible since their Young's modulus is very high (0.9 to120 5.5 TPa) [14]. When a compressive stress is applied to the composite, the compressibility of the matrix leads to a decrease in the inter-particle distance of the MWCNT. This forms close conducting paths, which result in a decrease in

the resistance of the composite i.e. NPC effect. When the magnitude of the stress exceeded the yield stress, a PPC effect could be seen.

Stresses above the yield stress caused orientation of the MWCNT in the transverse direction, buckling or breakdown of MWCNT and the destruction of the conducting path formed by MWCNT resulting in an increase in the composite resistance [14]. During cyclic loading, as shown in Figure 16, the specimen resistance (DC measurement) undergoes an increase and decrease with stress on the sample.

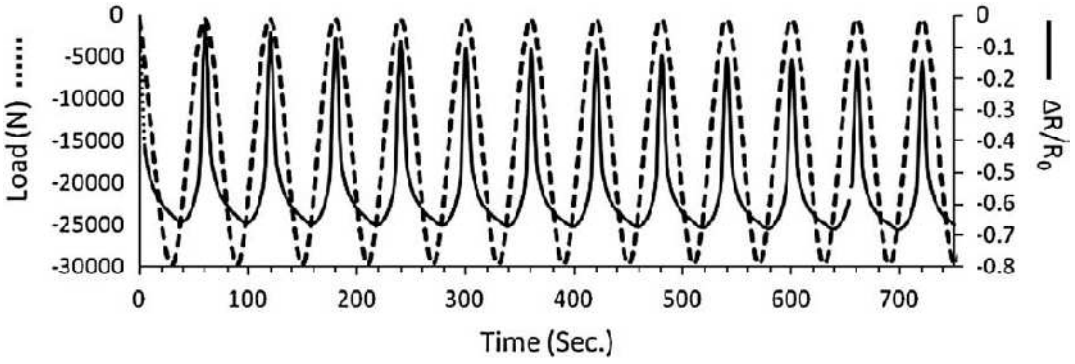

Figure 16: Resistance measured under cyclic loading.

The decrease in resistance was observed with increasing time at unloading condition due to time dependency of piezoresistance or building up of some permanent residual stain after every cycle of loading. The resistance sharply decreased under the instantaneous application of the compressive stress.

Under constant load, there was a negligible change in resistance over time. This correlated to the increase in conductivity on load application and the consequent decrease

in resistance. Similar measurements were also performed on two 4% PVDF samples under loading conditions. The PVDF strands were subjected to increasing loads and measurements of resistance were recorded using the NERAC system. Figure 17 shows the behavior of the resistance with increasing load.

Lastly, the NERAC board was used to record resistance measurements from a sample of undamaged smart concrete. Baseline readings were recorded with the NERAC

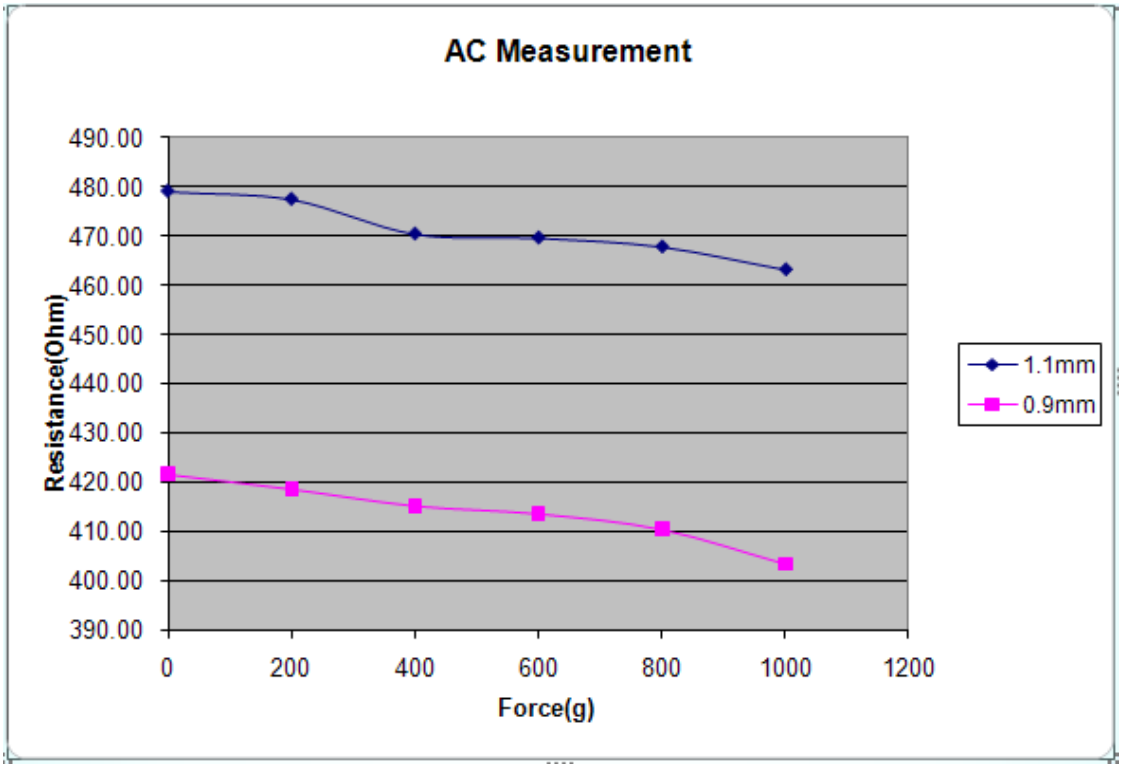

Figure 17: Resistance measurements from PVDF samples using NERAC unit.

and the digital multimeter. No significant difference was observed for baseline resistance readings using the DC and AC methods, respectively. Subsequently, two samples of

smart concrete were subjected to cyclic loading using the MTS system and measurements were taken using the NERAC board. The experimental set-up is shown in Figure 14. The concrete sample was subjected to cyclic loading in the MTS apparatus and DC measurements were effected using the NERAC board. The resistance values were measured for two other source currents. The data showed consistent behavior. The resistance data has been converted to a dimensionless quantity called relative resistivity given by $(R-R_O)/R_O$ [14, 16]. Prabhakaran [16] has shown that this ratio is proportional to strain and can be used to model damage in composites.

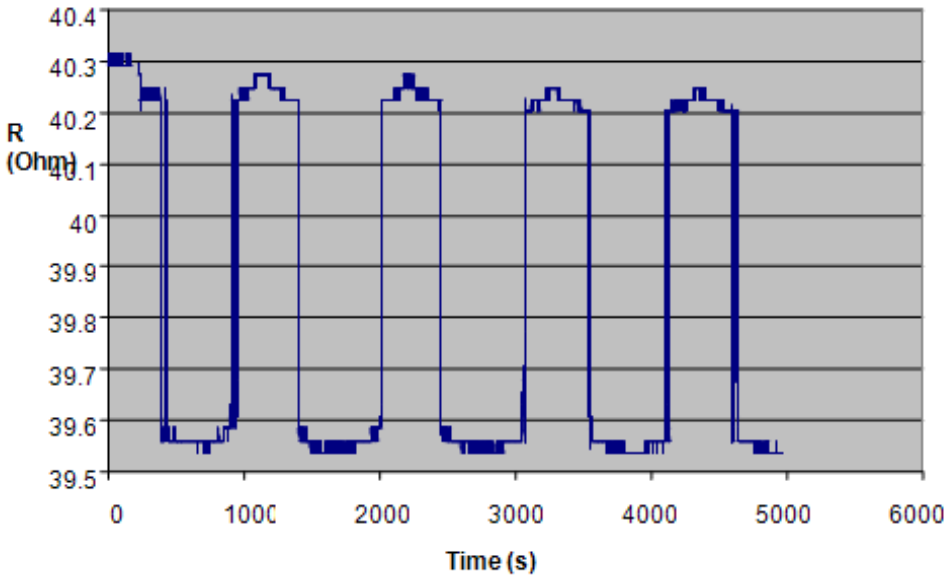

Figure 18: Resistance measurement on concrete sample using DC source current under loading conditions.

The results from this study corroborate the results obtained by D.D.L Chung et al [17] from their studies on smart concrete. When the smart concrete specimen is subjected to cyclic loading, it leads to a mechanism that involves the discontinuous carbon fiber

used as an admixture in the smart concrete, bridging micro-cracks and getting slightly and reversibly pulled out upon tension. This causes a reversible increase in the measured resistance. The reverse occurs on compression [17]. Strain is measured with a conventional strain-meter (Omega) to show the existing correlation between strain and resistance. The resistance increases reversibly upon tensile loading and decreases reversibly upon compressive loading. Figure 18 displays the behavior of the normalized resistance with cyclic load for DC source current of 28 mA. Results from AC measurement under load conditions using the MTS machine are presented in Figure 19.

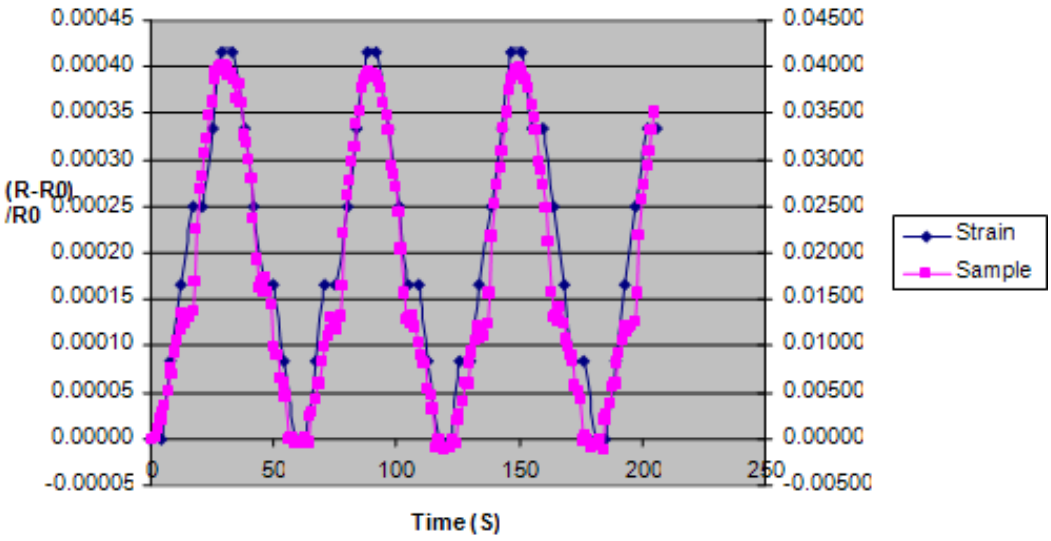

Figure 19: Measurement of normalized resistance and strain for AC current of 14.8 mA at 1 KHz.

The NERAC board was set up for AC measurements at a frequency of 10 KHz. Figure 20 shows raw data measured and its variation with respect to time. Four-probe technique was used to record the resistance of the concrete sample using the NERAC,

simultaneously strain measurements were obtained using an advanced capability strain meter.

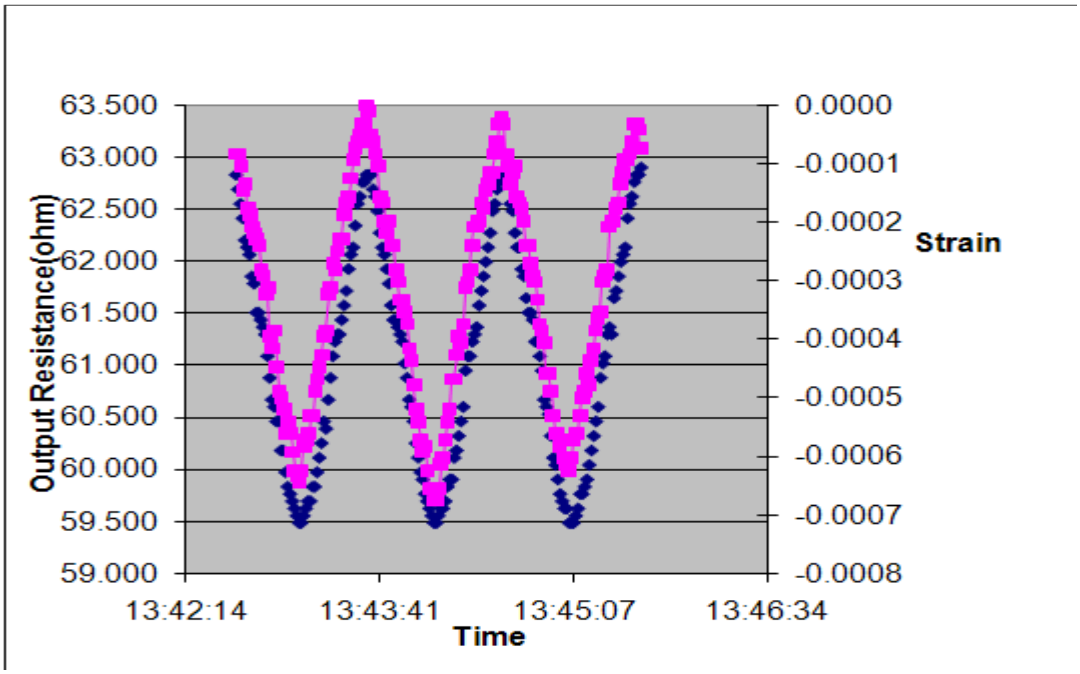

Figure 20: AC Measurement for source current of 8.56 mA source at 10 KHz was able to replicate similar measurements at SUNY with advanced Keithly multi-meter.

5.2.2.2.Damage Effects

A composite panel of a helicopter blade was the subject of damage tests. In the first set of experiments, the panel was subjected to increasing force and the resistance was measured using four-probe, DC method with the NERAC unit. The resistance increased with increase in force as shown in Figure 21. AC measurement followed a similar pattern, with statistically insignificant variation between the two measurements. The results obtained from damage studies corroborate the findings of Chung et al. [18]. In

their investigations, Chung et al. [18] have shown that upon major damage, all resistances abruptly and irreversibly increase, such that the onset occurs earlier for the compression surface resistance and the oblique resistance than the tension surface resistance. This was further borne out by the second set of experiments performed on the composite panel.

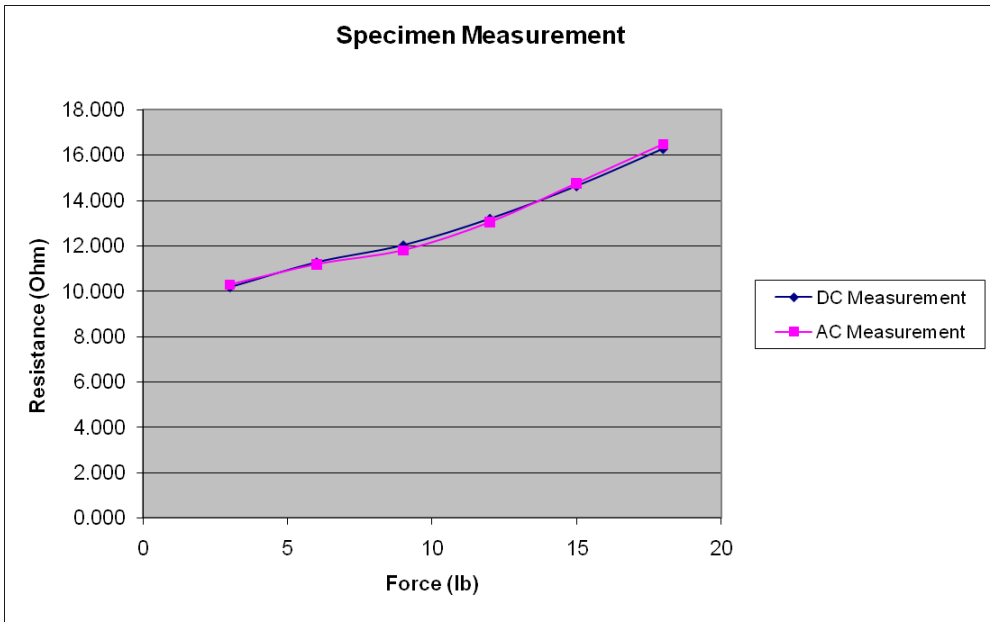

Figure 21: DC and AC measurement on composite panel subjected to varying loads (weights).

In order to induce damage in the sample, holes were drilled using a power drill and the resistance was measured with the NERAC unit. A graph of the variation in resistance with number of holes – signifying increased damage, showed an increase in resistance. The measurements from the NERAC unit closely followed measurements recorded from the HP multi-meter, as shown in Figure 22 with data in Table 1 for DC

method and Figure 23 with data in Table 2 for AC method. The resulting measurements did not show a statistically significant (95% confidence) deviation.

		Digital Multimeter Measurement		NERAC System Measurement	
Hole(s) Drilled	Current Supply (A)	DC Measurement	DC Resistance (Ohm)	DC Measurement	DC Resistance (Ohm)
1	0.01556	0.421	27.057	0.422	27.121
2	0.01556	0.433	27.828	0.431	27.699
3	0.01556	0.439	28.213	0.438	28.149
4	0.01556	0.443	28.470	0.443	28.470
5	0.01556	0.455	29.242	0.456	29.306
6	0.01556	0.463	29.756	0.462	29.692
7	0.01556	0.472	30.334	0.47	30.206
8	0.01556	0.475	30.527	0.478	30.720

Table 1: Damage effect using DC measurement method (data for figure 22).

		Digital Multimeter Measurement		NERAC System Measurement	
	Current Supply (A)	AC Measurement	AC Resistance (Ohm)	AC Measurement	AC Resistance (Ohm)
1	0.01574	0.456	28.971	0.455	28.907
2	0.01574	0.463	29.416	0.463	29.416
3	0.01574	0.468	29.733	0.469	29.797
4	0.01574	0.472	29.987	0.47	29.860
5	0.01574	0.477	30.305	0.474	30.114
6	0.01574	0.489	31.067	0.485	30.813
7	0.01574	0.505	32.084	0.507	32.211
8	0.01574	0.511	32.465	0.516	32.783

Table 2: Damage Effect using AC measurement method (data for figure 23).

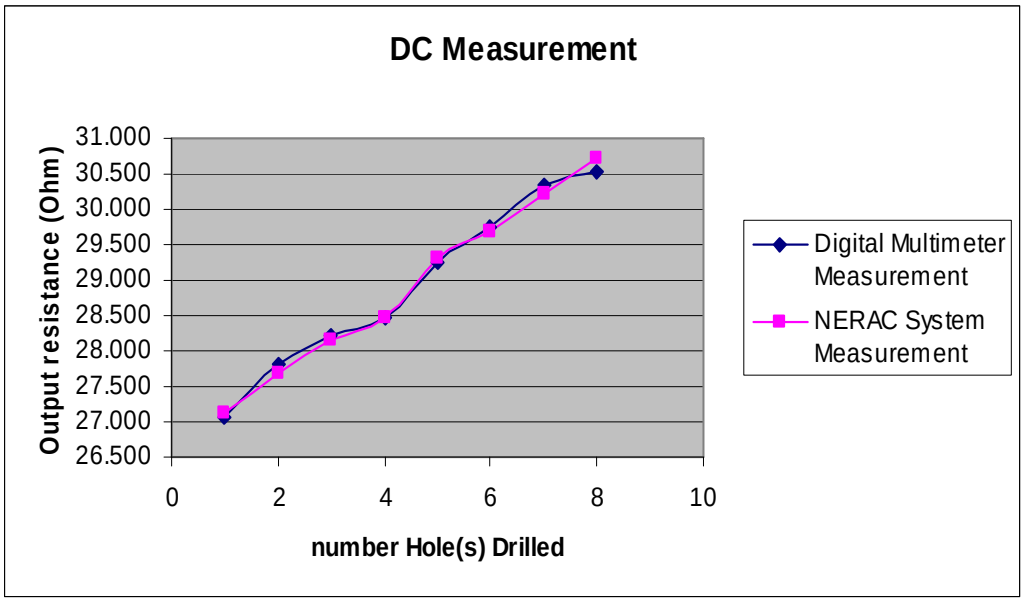

Figure 22: NERAC vs HP 1100 multimeter: Variation in resistance measured using DC measurement method NERAC with damage induced by drilling holes in the composite sample.

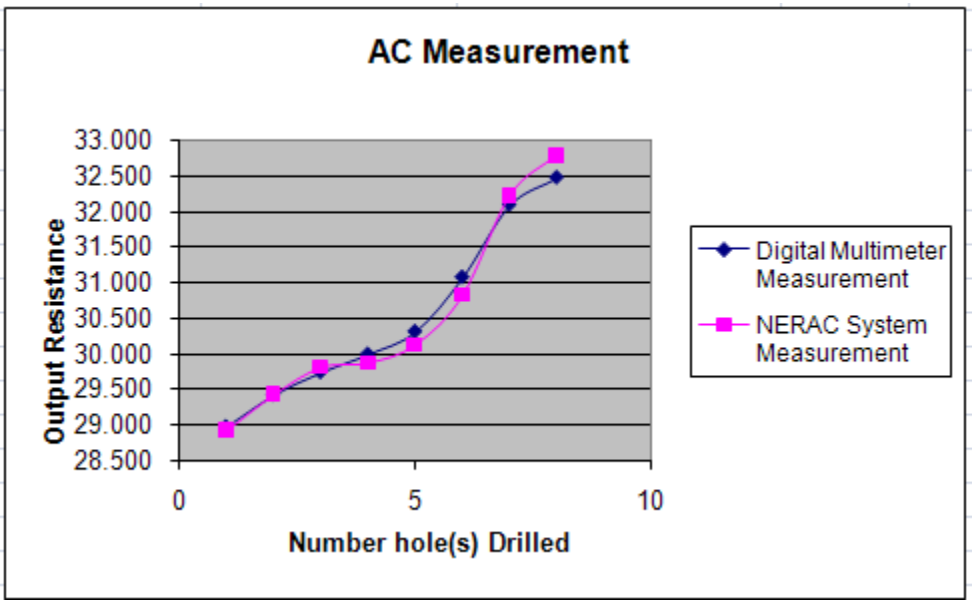

Figure 23: NERAC Vs HP 1100 multimeter: Variation in resistance measured using AC measurement method NERAC with damage induced by drilling holes in the composite sample.

CHAPTER 6

CONCLUSION AND RECOMMENDATION

6.1. Conclusion

Using resistance based measurements to assess damage in structural health monitoring holds great promise. To that end, the development of a microprocessor-based resistance monitoring system offers an intelligent, automated option. Given the increasing use of composites and carbon nano-tubes in development and design of structures, the NERAC unit facilitates assessing damage in engineering structures where damage is likely to originate at the material level and then progress to component and system level. AC measurement with variable frequencies seems to offer the best route to using resistance/impedance to determine damage in structures.

With small size, low weight, and multifunctional capability, NERAC System will deliver a high quality and convenience but less cost and apparatus system. NERAC device provides essential functions and accuracy data acquisition. The NERAC User Interface Tool is simple and comes with helpful instructions and features that would help user(s) to utilize it easily and could save them for data processing.

6.2. Recommendations

A basic conceptual of an electrical resistance-based self-sensing (NERAC) instrument has developed that opens a wide door for a practical NERAC's product accomplishment in the future. Future NERAC instrument will improve its functions to higher level with

- Frequency improvement: advance using Direct Digital Synthesis (DDS) device such as AD9835 from Analog Devices to acquire higher and more precise frequency.
- Analog inputs: redesign amplifier circuits to allow NERAC handle higher input voltage. Also NERAC System can accept 4 set of measurement inputs simultaneously
- Redesign frequency meter get more accurate reading and handle fully from minimum to maximum frequency
- The current NERAC possesses one set of electrical contact for four-point resistivity measurement. To make the system practical, it is desired to development multiple sets of electrical contacts.

6.3. Other Challenges

There exists a huge challenge in surface electrical contacts (electrodes) development, which can work in a robust fashion for practical applications.

APPENDIX A

CIRCUIT DESIGNS

Appendix A explains more detail about design and operating function of each function block in Figure 5.

A1. Power Supply

A1.1. 3.3 V – Voltage Regulator

Figure A1 shows a regulated 3.3V, which is stepping down from a 15V voltage source using a LM2575 chip from National Semiconductor. This chip "offers a high-efficiency replacement for popular three-terminal linear regulators. It substantially reduces the size of the heat sink, and in many cases no heat sink is required" [19]. Output current of the LM2575 can supplies up to 1A. This current is guaranty to be stable when the MCU resources are fully used and operating at maximum speed. In Figure A1, C_{out} together with a 330µH "defines the dominate pole-pair of the switching regulator loop" [19]. Diode D1 has a current rating of 1.2 times higher than maximum output current and this will help to prevents unexpected current short at output. C_{in} is a 100µF connected close to the device input for filtering and stabilizing the LM2575's operation. The 3.3V output at the 330µF C_{out} is regulated, but a filter is added at the output still necessary since it is supplying voltage to the microcontroller. Also, in Figure A2, VA and VDD decoupling capacitors are connecting in parallel after the filter to assure clean DC voltage supplies to VDD, VS, and VA of the microcontroller.

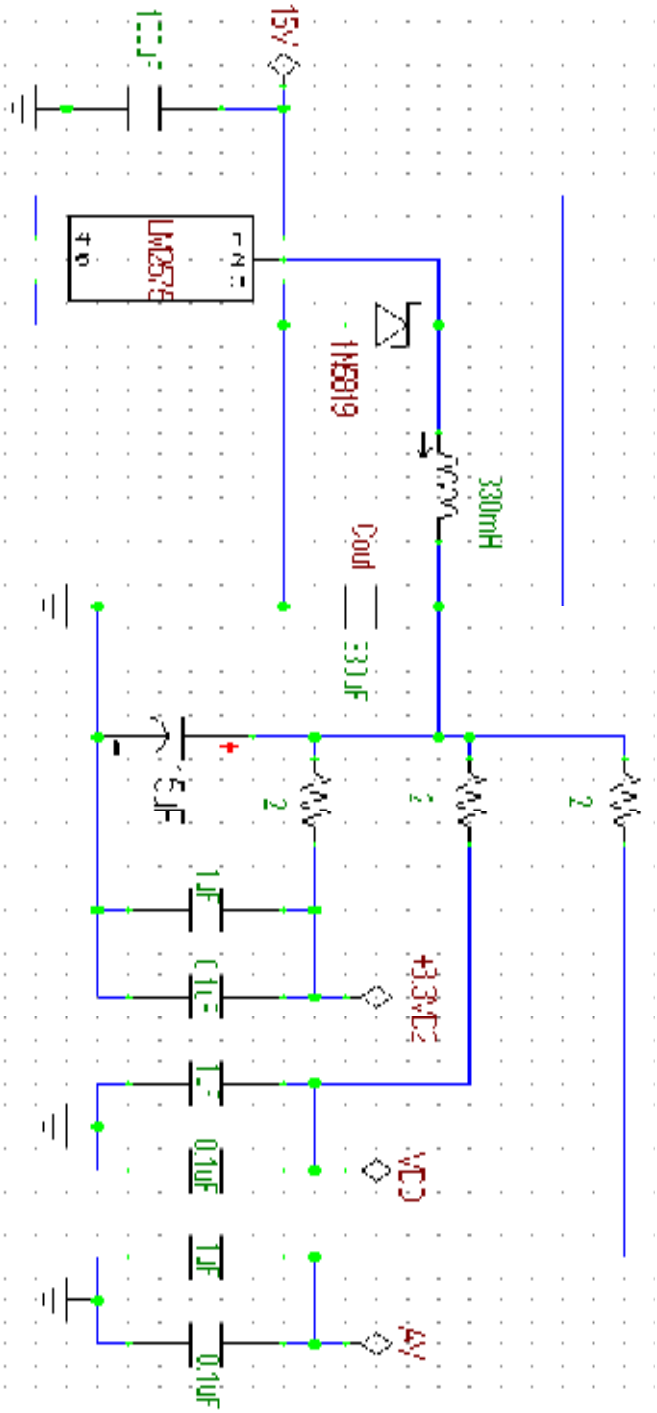

Figure A1: Regulated 3.3 V step down voltage.

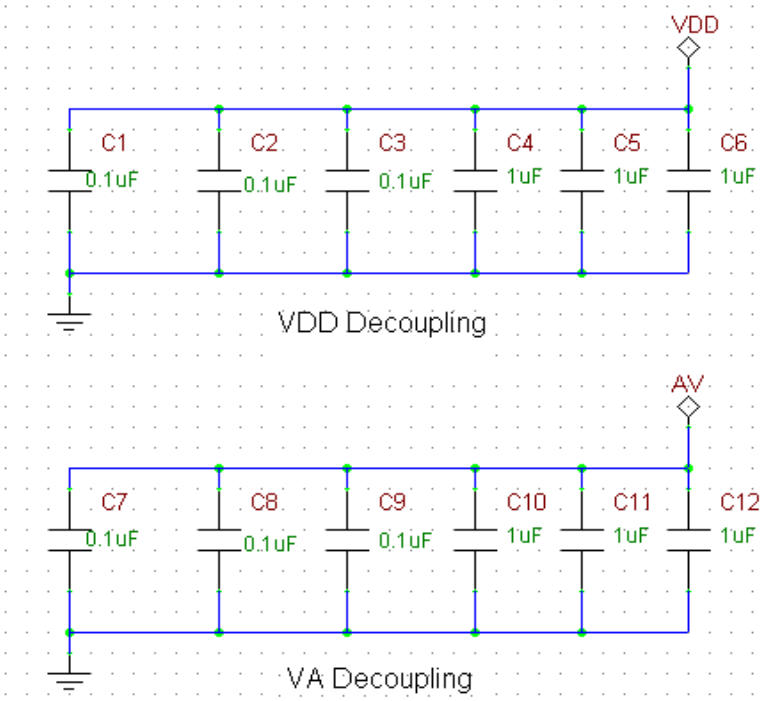

Figure A2: Decoupling capacitors circuits.

A1.2. Voltage Inverter

The operation of circuit in Figure A3 is -Output = Input with output current is less than 200mA. Two 10µF capacitors are used for filtering

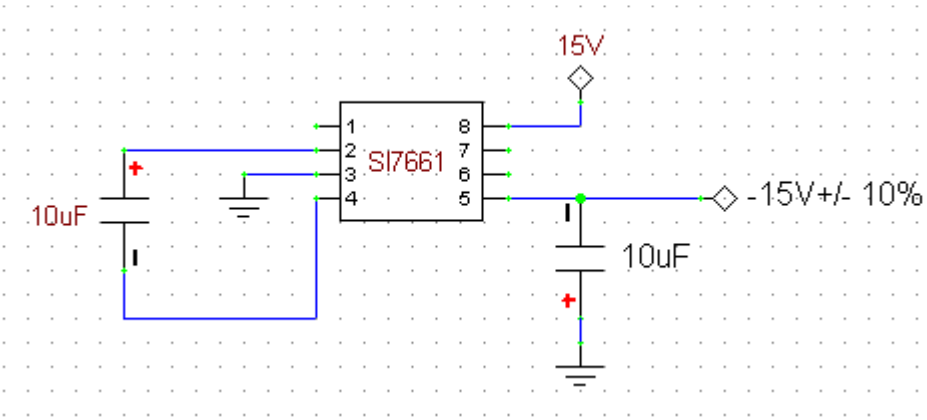

Figure A3: SI7661 200mA voltage inverter.

A2. C8051F040 Microcontroller

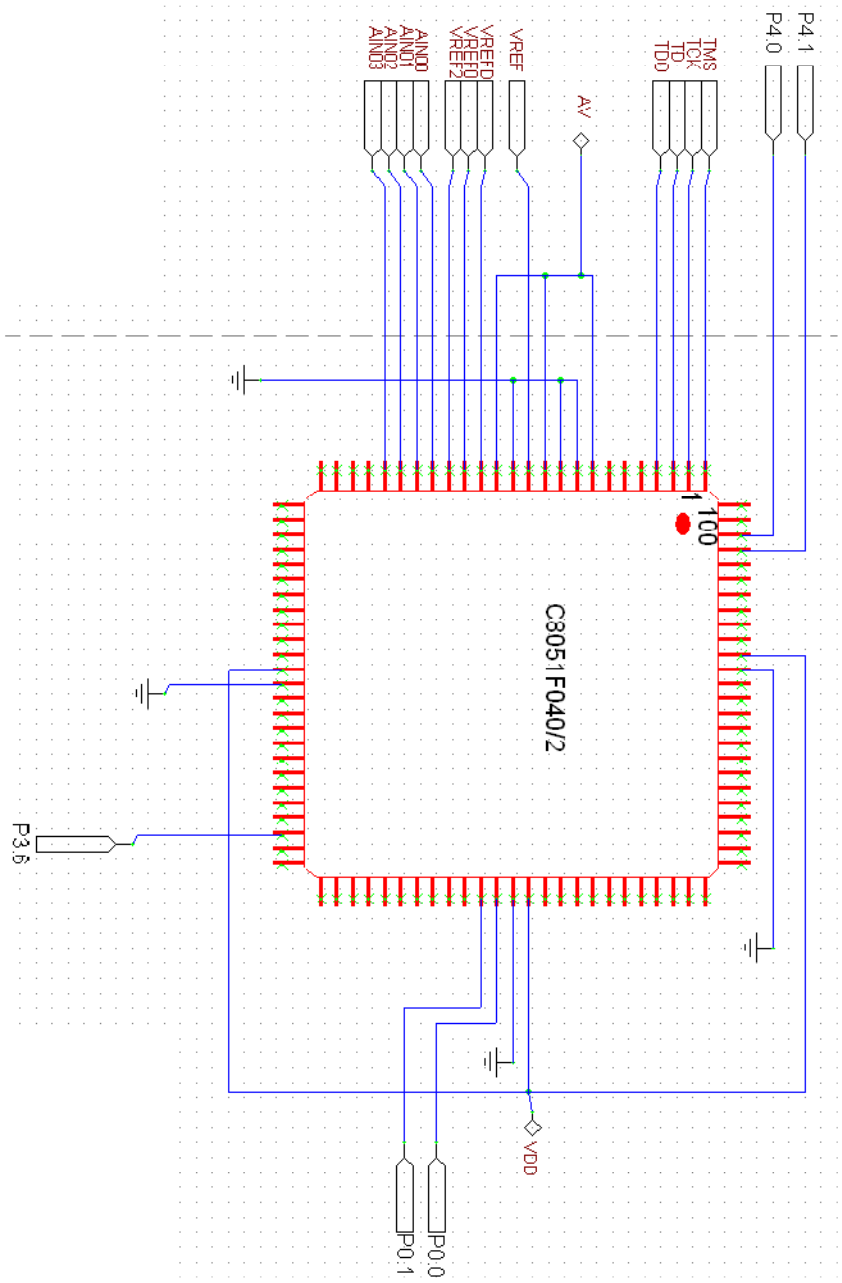

Figure A4: C8051F040 microcontroller unit.

Figure A4 presents pin connection to and from MCU with external devices. Detail of pins configuration and function can be viewed at C8051F040 manufacture's datasheet [ref 20 and 21].

A3. JTAG Connection

Figure A5 is a 10 pins JTAG connection. The 4.7kΩ in the circuit limits the current flow to MCU's TCK and pin 4 of a debug adaptor.

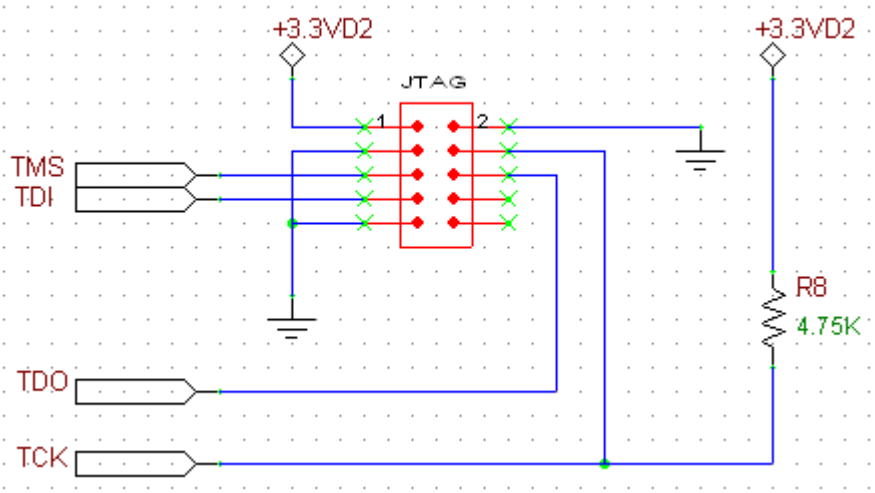

Figure A5: JTAG Connection.

A4. Serial (RS-232) Signal Amplifier

The original RS-232 signal amplifier that Silabs Inc, use in their C8051F040 development board is a SP3223E chip from SiPex. I replaced that chip with a MAX3223 from Maxim-IC for higher energy efficiency. The pin configuration of SP3223E and MAX3223 are the same, and a circuit diagram of serial RS-232 connection using MAX3223 is in Figure A6.

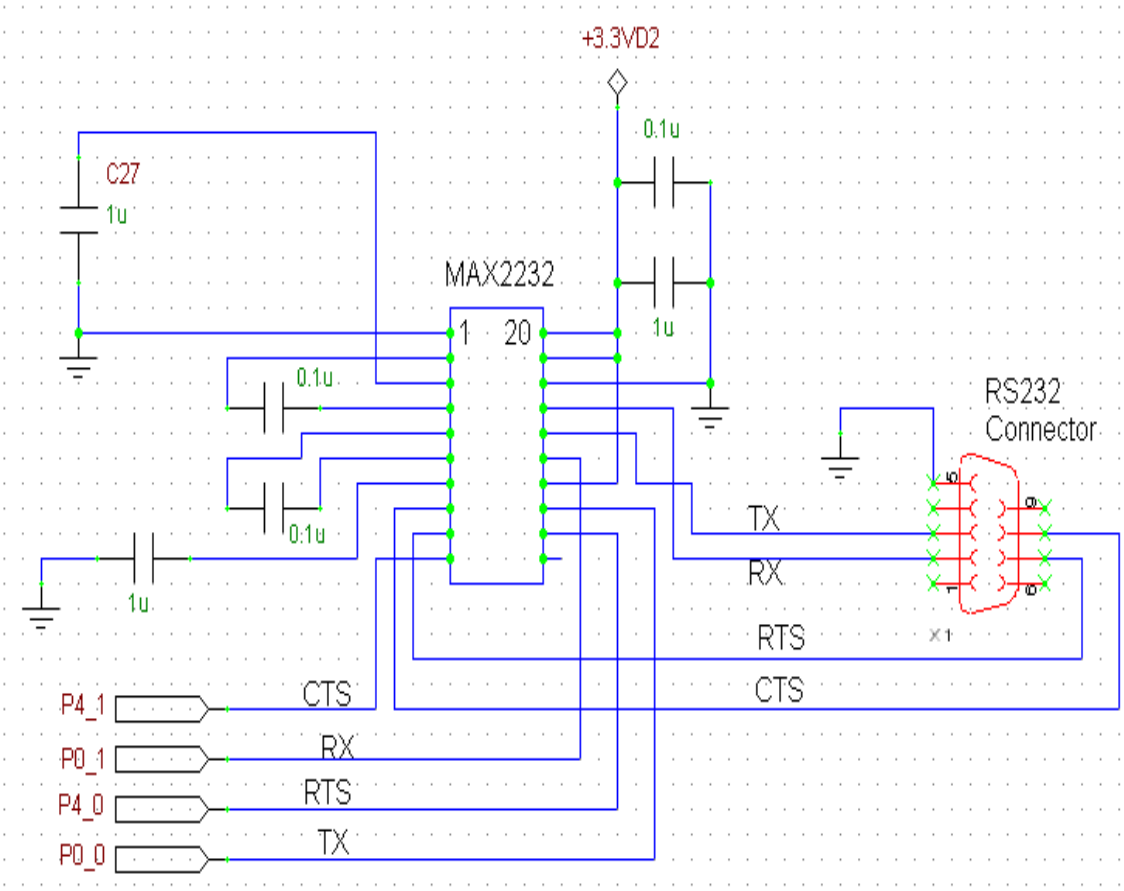

Figure A6: RS232 signal amplifier.

A5. Voltage References

Figure A7 shows a voltage reference circuit. Capacitors C19, C22, and a 33nF capacitor from the LM4120 stabilize and filter any AC components such as noise before supply to MCU Vref pin. 2.4V or 3V reference is selected by inserting a jumper to a four pins conn header.

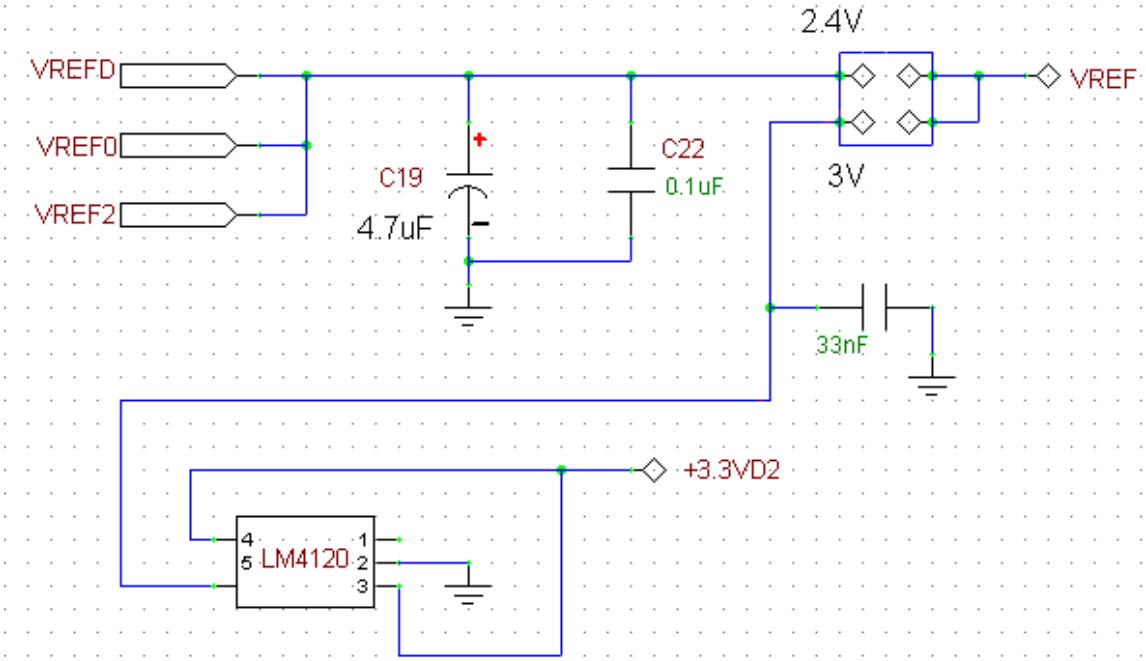

Figure A7: Voltage references.

A6. Power Indicator

This circuit simply indicates if NERAC's power is ON or OFF state. In Figure A8, a 470Ω resistor connect in series with a LED to limit current flow to the LED.

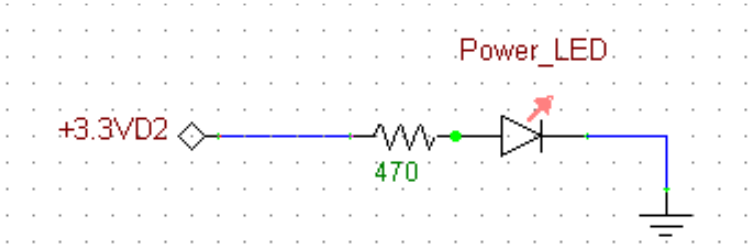

Figure A8: Power indicator.

A7. Regulated DC Current Source

DC current Source supplies constant DC current to load regardless of changing of load resistance. This DC current is adjusted by varying a 100Ω for flexible current range. Figure A9 shows a simple but effective current source circuit by using a LM317 [27]. The output current is:

$$I_{out} = \frac{1.25V}{R} \qquad \text{(A1)}$$

Where R = 20Ω + (100ΩPOT)

Hence, current range for this particular design is from 10mA to 62.5mA

Input of the LM317 is a 15V voltage source; therefore, the output current to Load is limited to the equation A2:

$$I_{out} < \frac{15V}{R_{Load}} \qquad \text{(A2)}$$

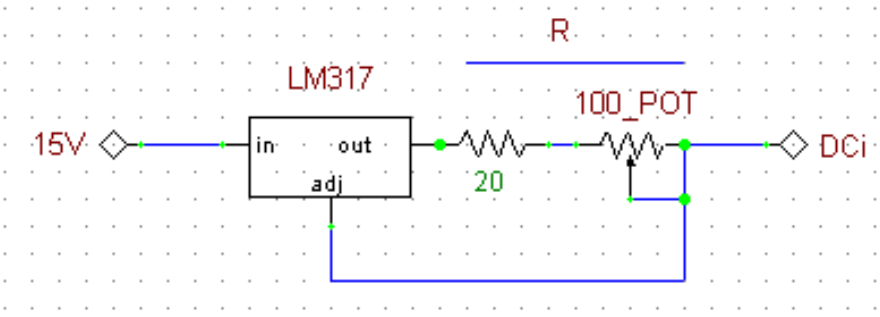

Figure A9: Regulated DC current source circuit.

A8. Regulated AC Current Source

The AC current source in the NERAC device consists of two circuits: a Sine Wave Generator circuit and a current amplifier and regulator circuit.

A8.1. Sine Wave Generator

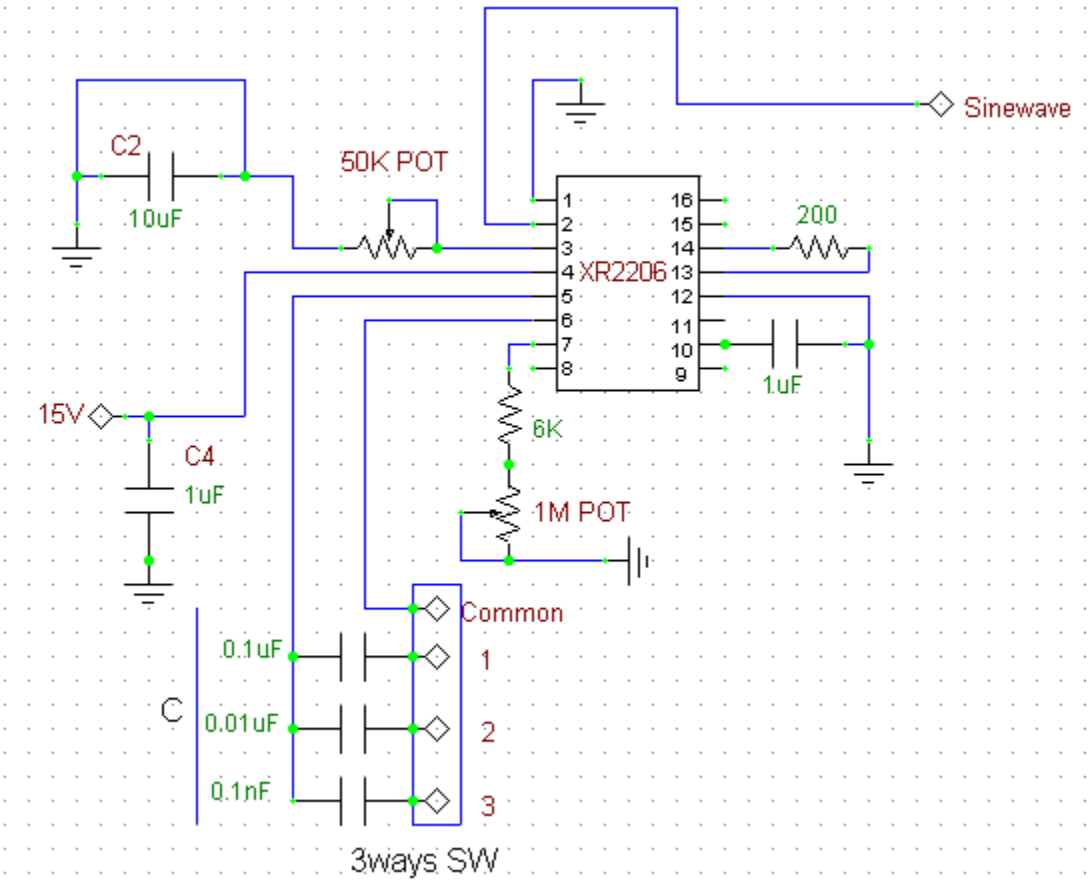

Figure A10: Sine Wave Generator.

Figure A10 shows a sine wave generator circuit using XR2206 chip [22]. Vcc input of this chip is a 15V DC at pin 4 and output is an AC sinusoidal signal at pin 2. The frequency of sinusoidal signal is calculated:

$$F = \frac{1}{RC} \qquad \text{(A3)}$$

Where R = 6 KΩ + 1M ΩPOT

C is the selection of 0.1µF, 0.01µF, or 0.1nF

Therefore, the frequency ranges from 10Hz to 1.6MHz

A8.2. AC Current Amplifier and Regulator

Figure A11 continues from Figure A10. Sine wave signal passes through a 220µF polarized coupling capacitor to eliminate any possible present of DC component before amplified by the op amp AD827. The gain of the amplifier is adjusted from 1 to 3.5 by a 25 KΩ POT, which also adjusts the output current. Vp-p (Sinewave1) output at pin 7 of the AD827 is presented in equation A4

$$\text{Sinewave1 (Vp-p)} = -\frac{10k\Omega + 25k\Omega\ POT}{10k\Omega} * 4\text{Vp-p} \qquad \text{(A4)}$$

Sinewave1 signal continue through a voltage control current source (VCCS) to be regulated. The concept of a VCCS circuit is that current controlled by input voltage. If ACH and ACL are connected to two ends of a sample, the current flow through that sample will be:

$$I = \frac{Sinewave1_{rms}}{R} \qquad \text{(A5)}$$

Where $Sinewave1_{rms} = 0.3535 * Sinewave1Vp-p$

R is selected resistor of 1KΩ or RGAIN

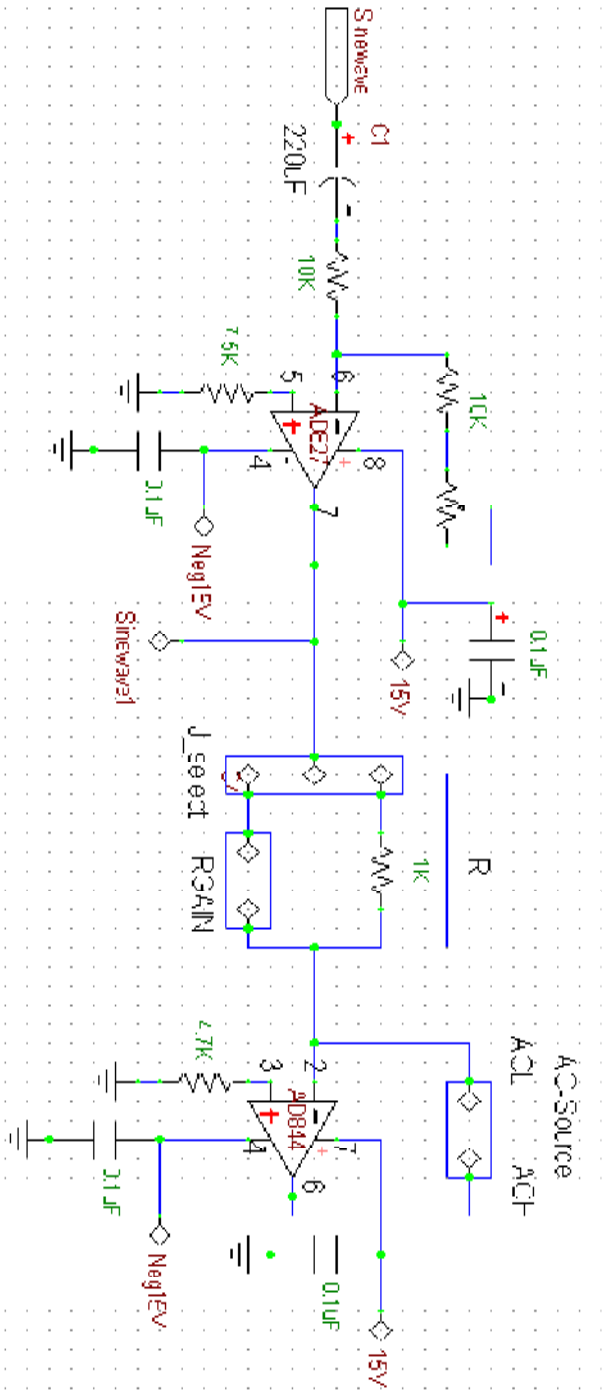

Figure A11: Regulated AC current with gain adjustable.

Equation (A5) shows that current is only reflected by two criteria, and they are $Sinewave1_{RMS}$ (input voltage) and R. Therefore, current will not change if sample resistance change. The limitation of this VCCS is that the value of R must be greater than sample resistance. Therefore, for samples resistance that greater than 1KΩ, supply current will not reach up to 10mA

A9. AC to DC Converter

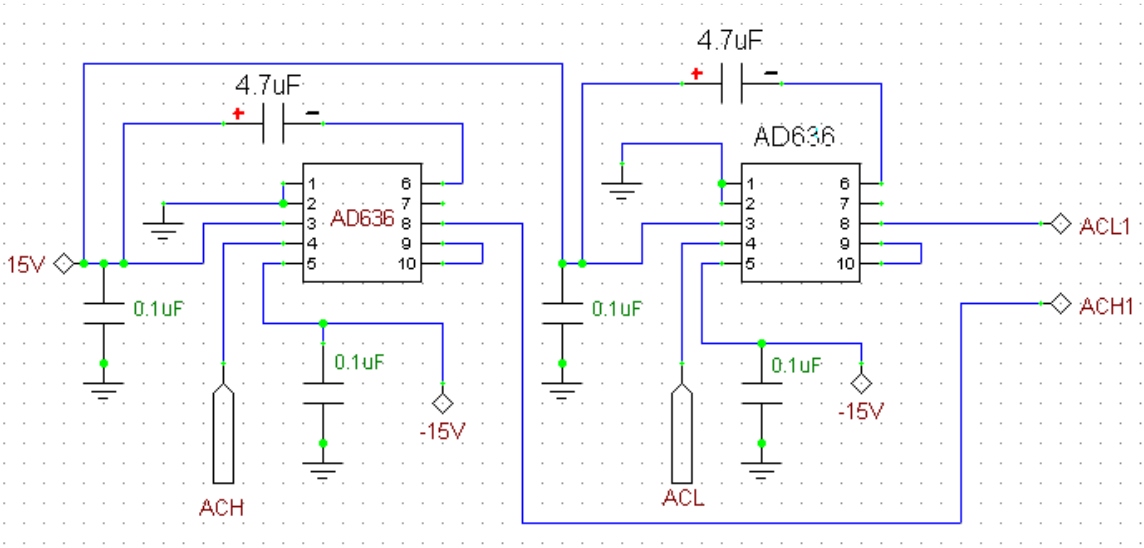

Figure A12: AC to DC converter.

Figure 12 shows a simple but accurate of 2 RMS to DC converters circuit using AD636 chip from Analog Devices. “The AD636 computes the rms of both ac and dc signals. If the input is a slowly varying dc voltage, the output of the AD636 tracks the input exactly. At higher frequencies, the average output of the AD636 approaches the rms

value of the input signal. The actual output of the AD636 differs from the ideal output by a dc (or average) error and some amount of ripple, as demonstrated in Figure A13" [23] with frequency response described in table A1.

AD636 requires only one external component and that is a 4.7 µF capacitor. Inputs are AC signal at pin 4 and outputs are DC signal at pin 8. Output DC signals are a true RMS of AC inputs and expressed in the following equation:

$$V_{OUT} = V_{IN}RMS \qquad (A6)$$

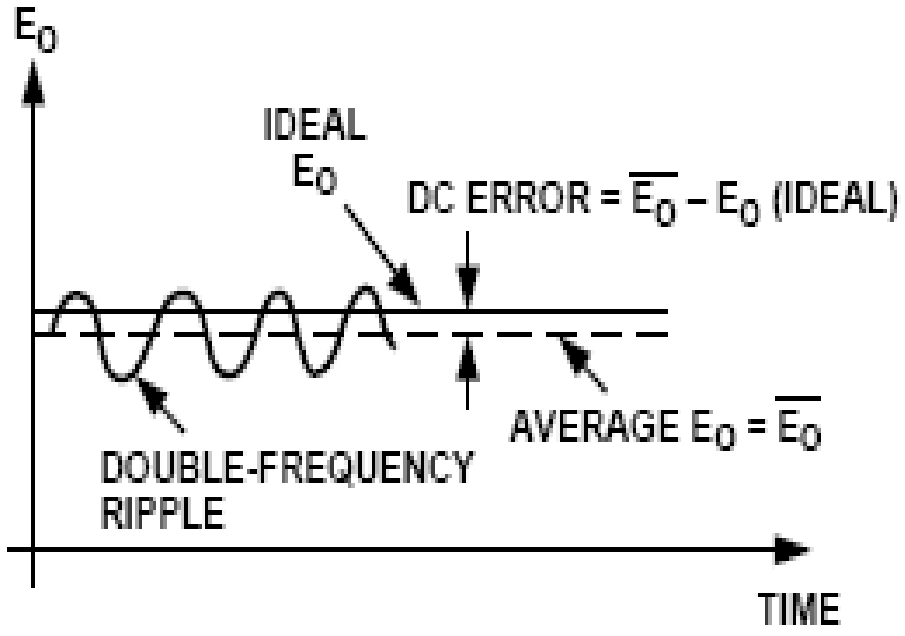

Figure A13: Typical output waveform for sinusoidal input [23].

Gain (dBm)	Frequency
0 dBm	5 Hz to 380 kHz
−10 dBm	5 Hz to 370 kHz
−20 dBm	5 Hz to 240 kHz
−30 dBm	5 Hz to 100 kHz
−40 dBm	5 Hz to 45 kHz
−50 dBm	5 Hz to 17 kHz

Table A1: Frequency response of AD636.

A10. Instrumentation Signal Condition

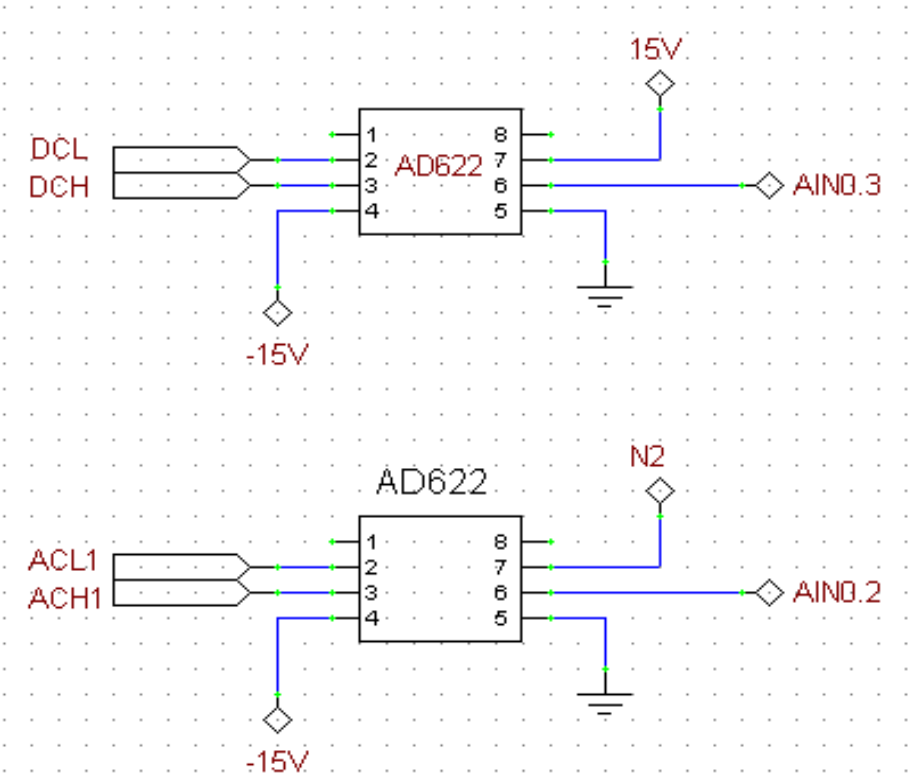

Figure A14: Instrumentation signal conditioning circuits.

Figure A13 shows the connections of two instrumentational op amps AD622. Pins number 1 and 8 of an AD622 are for output gain. In this application, gain is not necessary and thus, pin 1 and 8 are not connected. Circuit in figure A14 has a gain of one and outputs at pin 6 equal to:

$$AIN0.3 = DCH - DCL \qquad (A6)$$

$$AIN0.2 = ACH - ACL \qquad (A7)$$

A11. Sinusoidal to Pulse Converter

Circuit in Figure A15 simply converts a sinusoidal signal to pulse signal using a MMBT2222LT1 switching transistor from On Semiconductor. MMBT2222LT1 is a silicon transistor, therefore, it output level switch to LOW whenever sinusoidal signal amplitude greater than 0.6V. The 1KΩ resistor limits AC current to base terminal of the transistor and 200Ω resistor creates an I_C current of 3/200 = 15mA.

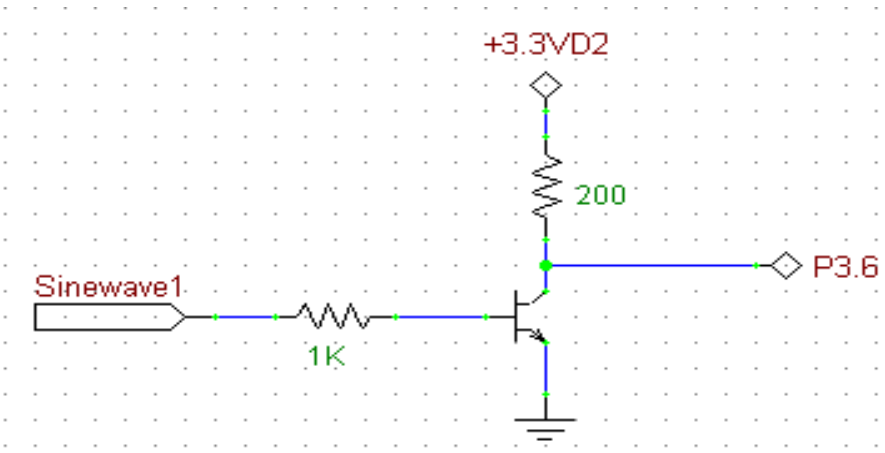

Figure A15: Sinusoidal to pulse converter.

A12. AC and DC Current Measurement

Figure A16 presents an AC and DC current to voltage converter. The output voltages of the circuit correspond to currents and described in the equation A8:

$$I = \frac{Vin}{Rshunt} \qquad \text{(A8)}$$

A12.1. DC Current Measurement

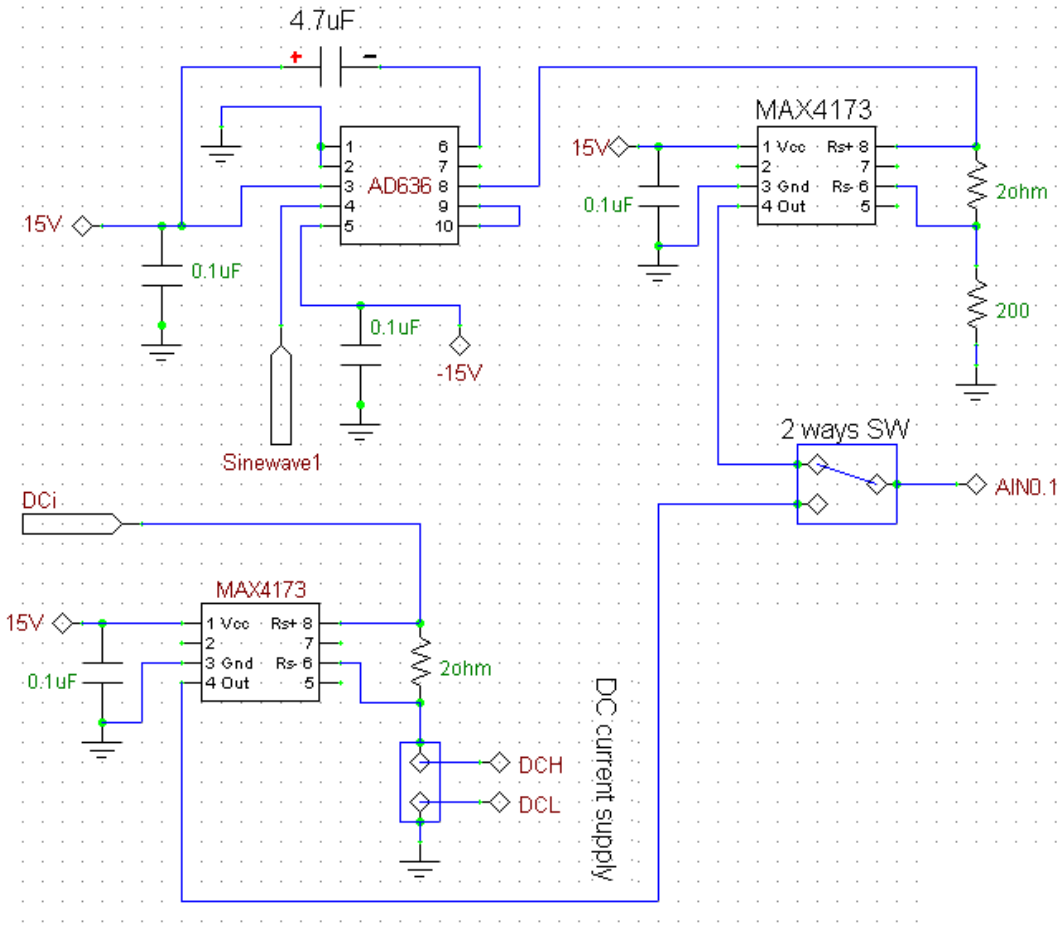

Figure A16: AC and DC currents measurement circuits.

Bottom section of circuit in Figure A16 is DC current measuring circuit using a current sense MAX4173 chip. DCi is an output current from DC current source connecting series with a 2Ω non-inductive shunt resistor and load. The MAX4173 measures voltage drop on the 2Ω resistor at Rs+ and Rs- and output that voltage at output's pin. The output voltage indicates the current flow, that is higher voltage drop between Rs+, and Rs- presents higher amount of current flows through that shunt resistor. According to Ohm's Law that current is the same at any cross-section of a series circuit. Thus, DC current is calculated using output voltage from the MAX4173:

$$I = \frac{Vout}{2\Omega} \qquad \text{(A9)}$$

A12.2.AC Current Measurement

The top section of Figure A16 is AC current measurement circuit. Its operating function follows:

- AC current converts to DC current using AD636
- A current sense chip MAX4173 measures that DC current.
- The measured DC current is multiplied with a variable to acquire true value of AC current.

Assume:

I = true AC current from an AC current source

I_{AC} = AC current measured using AC current meter

I_{DC} = calculated DC current from the chip MAX4173 using equation A9

X = Calibrated variable

Calibrated variable is the quotient of I_{AC} and I_{DC} :

$$X = I_{AC}/ I_{DC} \qquad (A10)$$

The true RMS AC current equal to

$$I = I_{DC}*X \qquad (A11)$$

A13. NERAC User Interfacing Tool (NUIT) Pages

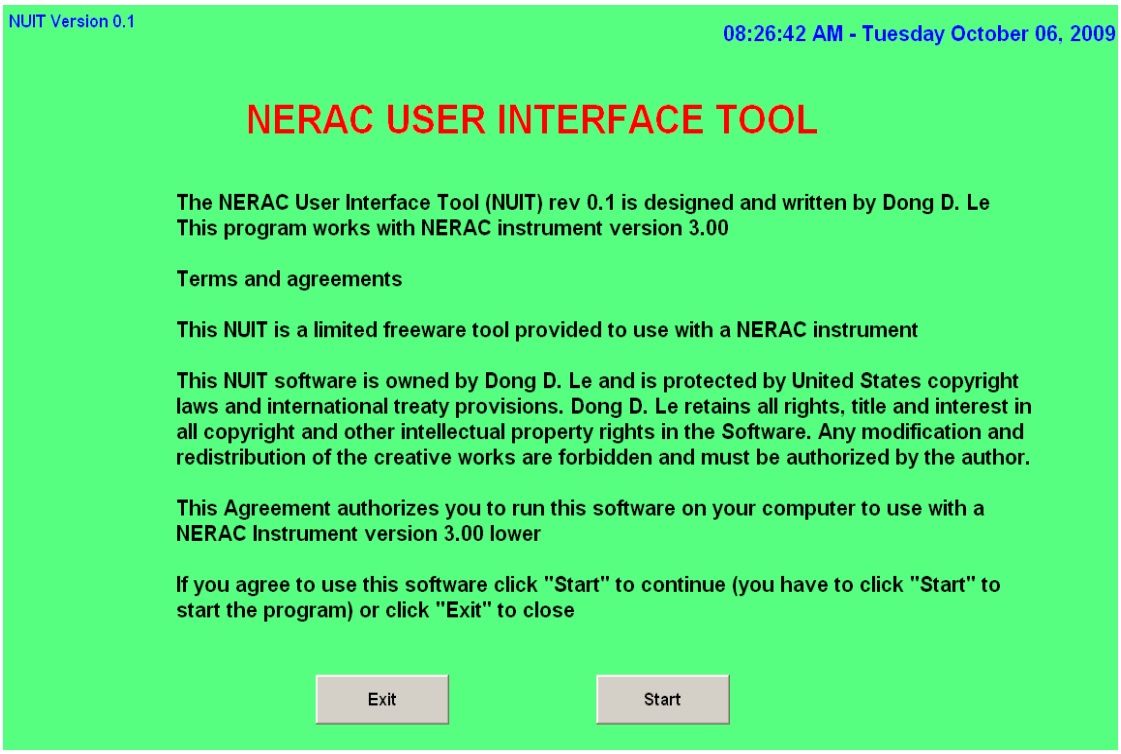

Figure A17: NUIT main page.

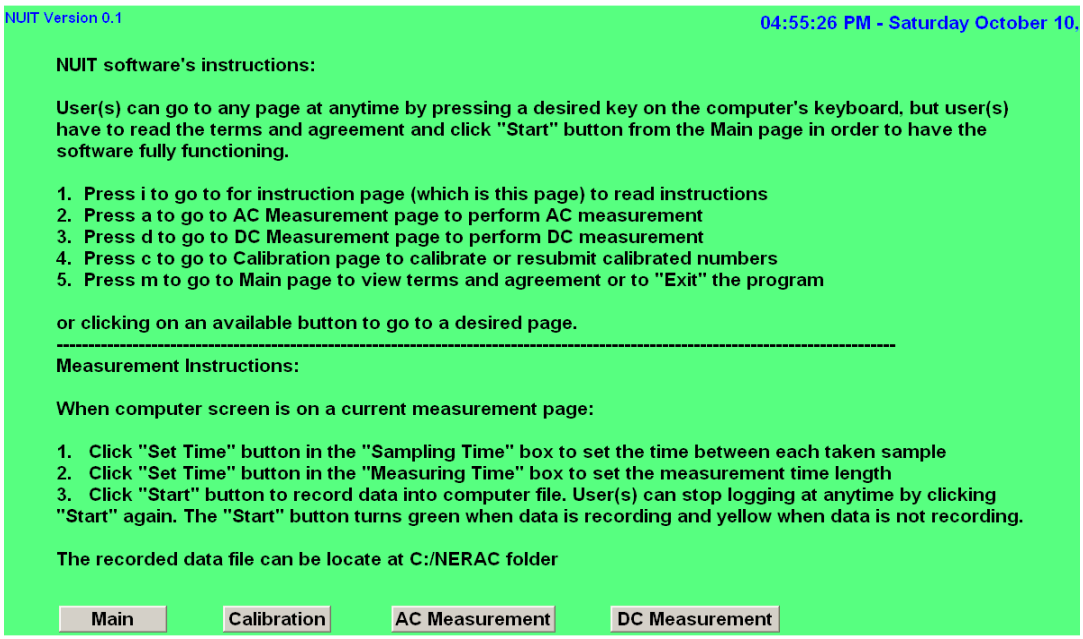

Figure A18: NUIT instruction page.

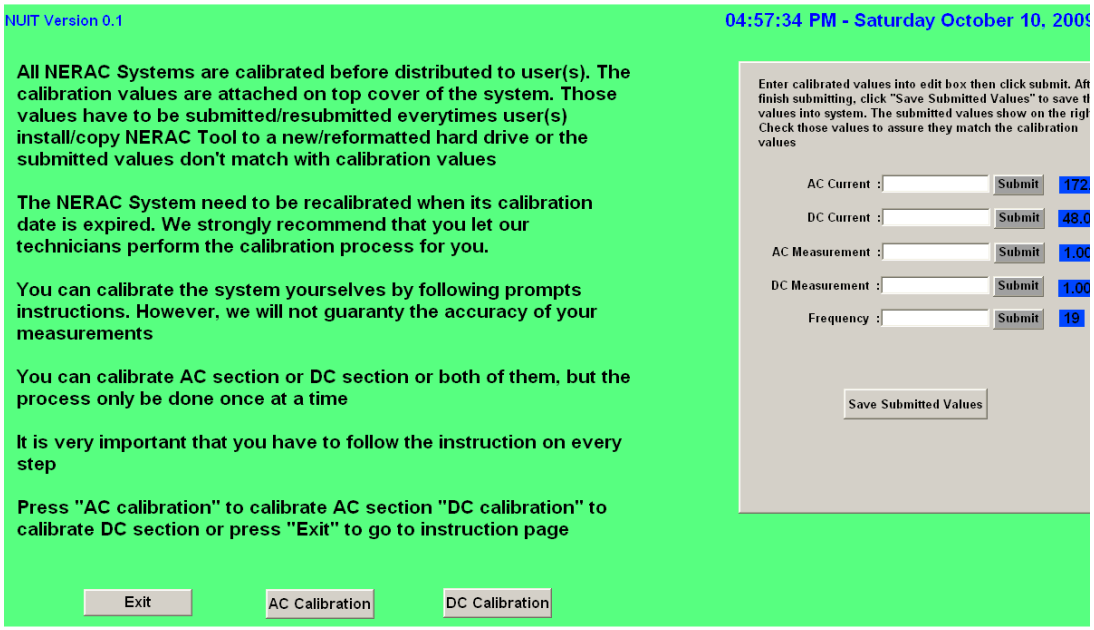

Figure A19: NUIT calibration page.

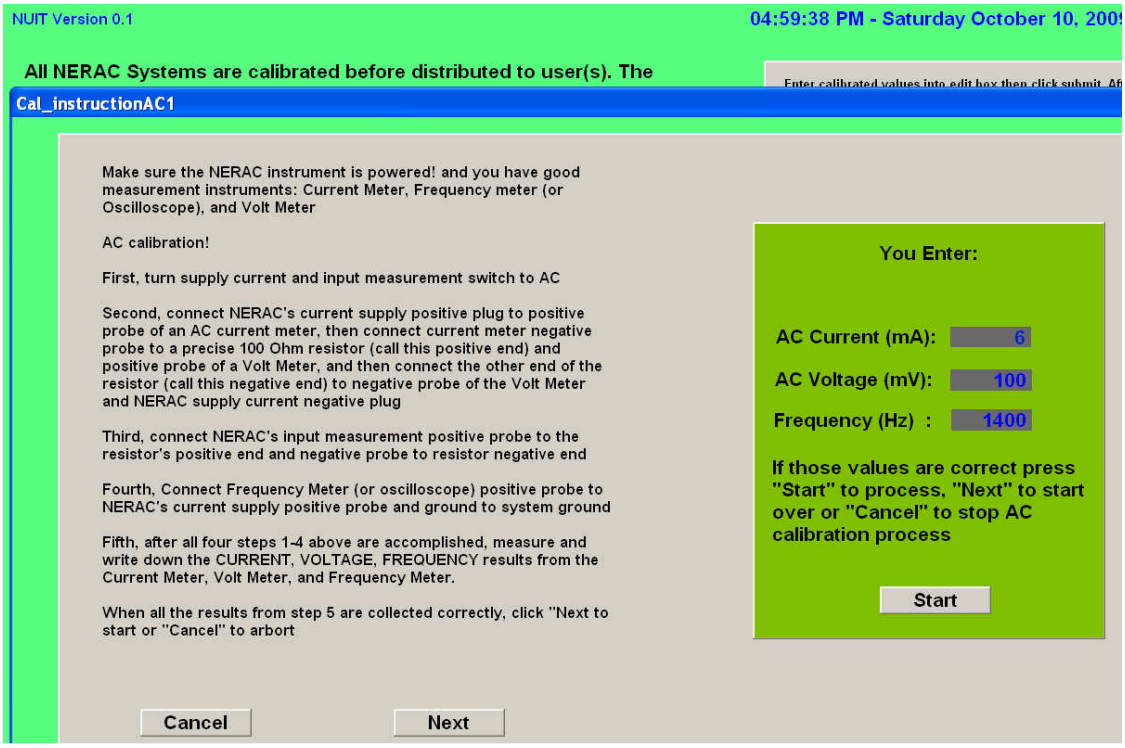

Figure A20: AC Calibration process pop up.

APPENDIX B

B.1. C8051F040 Microcontroller

Reference [21] is a data short of C8051F040 microcontroller

"Analog Peripherals

12-Bit ADC

- ±1 LSB INL; guaranteed monotonic
- Programmable throughput up to 100 ksps
- 13 external inputs; programmable as single-ended or differential
- Programmable amplifier gain: 16, 8, 4, 2, 1, 0.5
- Data-dependent windowed interrupt generator
- Built-in temperature sensor (±3 °C)

High-Voltage Differential Amplifier

- 60 V common mode input range
- Offset adjust from –60 to +60 V
- 16 gain settings from 0.05 to 16

8-Bit ADC

- Programmable throughput up to 500 ksps
- 8 external inputs; programmable as single-ended or differential
- Programmable amplifier gain: 4, 2, 1, 0.5

Two 12-Bit DACs

Three Comparators

Internal Voltage Reference

Precision VDD Monitor/Brown-out Detector

On-Chip JTAG Debug & Boundary Scan

- On-chip debug circuitry facilitates full speed, non-intrusive in-system debug (no emulator required)
- Provides breakpoints, single stepping, watchpoints, stack monitor, program trace memory
- Inspect/modify memory and registers
- Superior performance to emulation systems using ICE-chips, target pods, and sockets
- EEE1149.1 compliant boundary scan

Supply Voltage: 2.7 to 3.6 V

- Typical operating current: 10 mA at 25 MHz
- Multiple power saving sleep and shutdown modes

Temperature Range: –40 to +85 °C

High-Speed 8051 µC Core

- Pipelined instruction architecture; executes 70% of instructions in 1 or 2 system clocks
- Up to 25 MIPS throughput with 25 MHz system clock
- Expanded interrupt handler

Memory

- 4352 bytes data RAM
- 64 kB Flash; in-system programmable in 512-byte sectors (512 bytes are reserved)
- External parallel data memory interface

CAN Bus 2.0B

- 32 message objects
- ”Mailbox" implementation only interrupts CPU when needed

Digital Peripherals

- 64 port I/O; all are 5 V tolerant
- Hardware SMBus™ (I2C™ compatible), SPI™, and two UART serial ports available concurrently
- Programmable 16-bit counter array with 6 capture/compare modules
- 5 general-purpose 16-bit counter/timers
- Dedicated watchdog timer; bidirectional reset
- Real-time clock mode using timer 3 or PCA

Clock Sources

- Internal programmable 2% oscillator: up to 25 MHz
- External oscillator: Crystal, RC, C, or Clock

Package

- 100-pin TQFP (standard lead and lead-free packages)”

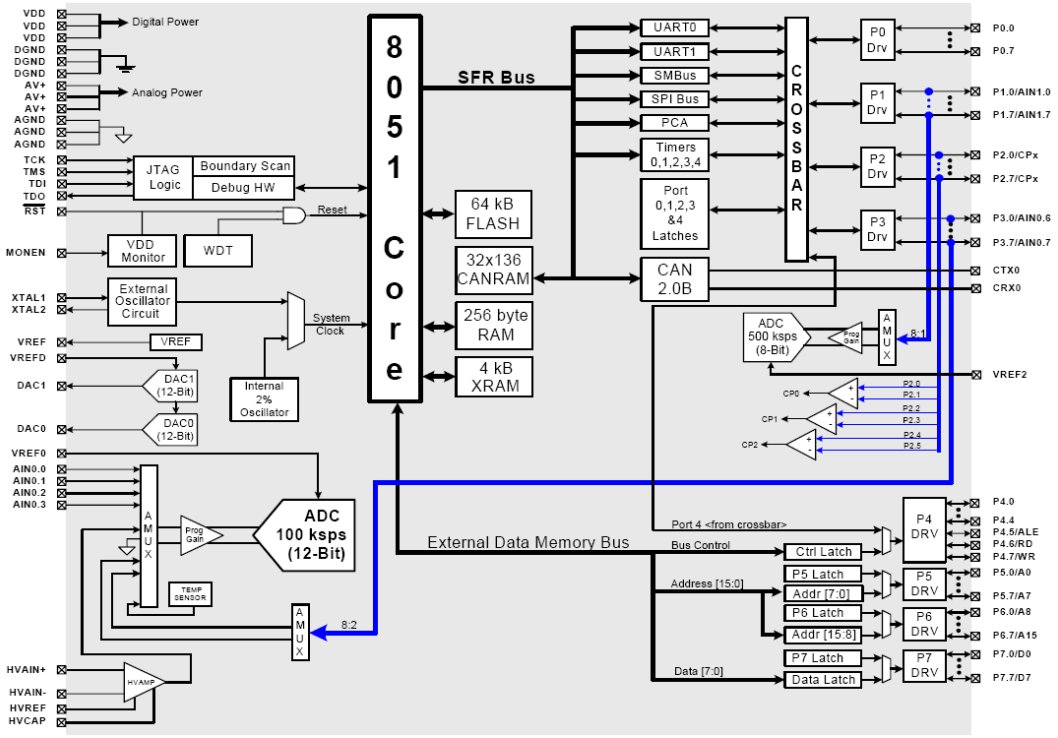

Figure B1: C8051F040 block diagram.

PARAMETER	CONDITIONS	MIN	TYP	MAX	UNITS
GLOBAL CHARACTERISTICS					
Supply Voltage		2.7		3.6	V
Supply Current (CPU active)	Clock = 25 MHz Clock = 1 MHz Clock = 32 kHz; V_{DD} Monitor Enabled		10 0.5 20		mA mA µA
Supply Current (shutdown)	Oscillator not running; V_{DD} Monitor Disabled		0.1		µA
Clock Frequency Range		DC		25	MHz
A/D CONVERTER					
Resolution			12		bits
Integral Nonlinearity				±1	LSB
Differential Nonlinearity	Guaranteed Monotonic			±1	LSB
Signal-to-Noise Plus Distortion		66	69		dB
Throughput Rate				100	ksps
Input Voltage Range		0		V_{REF}	V
D/A CONVERTERS					
Resolution			12		LSB
Differential Nonlinearity				±1	LSB
Output Settling Time			10		µs
COMPARATORS					
Supply Current	(each Comparator)		1.5		µA
Response Time	| CP+ – CP- | = 100 mV		4		µs

Table B1: C8051F040 electrical characteristics.

B.2. Silicon Laboratories IDE [Ref 26]

"The Silicon Laboratories Integrated Development Environment (IDE) is a complete, standalone software program that provides designers with all the tools they need to develop and test their projects. Figure B2 presents a Silicon Laboratory IDE window.

The features of the program include:

- Project Interface
- Full-featured, configurable Windows style editor
- Debugger - includes breakpoints, watchpoints, watch window, single step capability
- Tool Chain Integration - seamless integration of supported assemblers, compilers, and linkers.
- Customizable tool menu for integrating your own compiler, or other development tools.
- Configuration Wizard for generation of configuration code for a specified target environment"

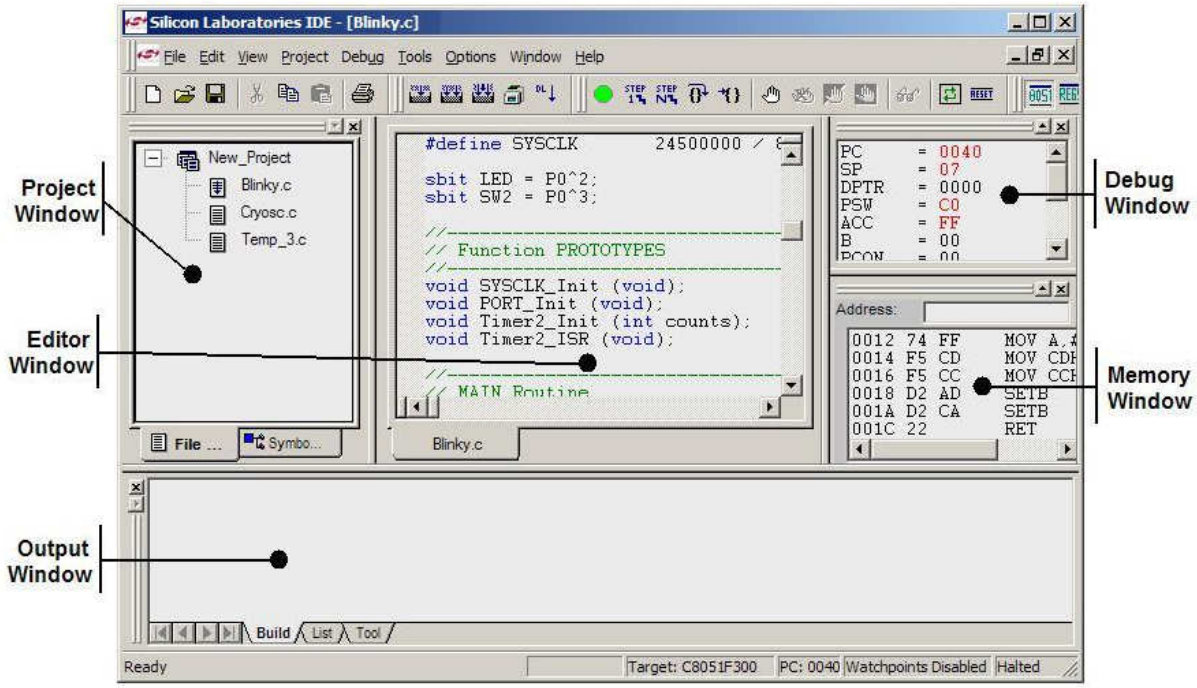

Figure B2: Silicon Laboratories IDE interface.

B3. Keil Development Tool [Ref 24]

"Keil development tools for the 8051 Microcontroller Architecture support every level of software developer from the professional applications engineer to the student just learning about embedded software development.

The industry-standard Keil C Compilers, Macro Assemblers, Debuggers, Real-time Kernels, Single-board Computers, and Emulators support all 8051 derivatives and help you get your projects completed on schedule".

B4. NERAC's MCU C Programming Codes

// NERAC.c

```
//    Dong D. Le
//    University Of North Texas
//    NERAC.c is modified from F04x_ADC0_ExternalInput_Mux.c
//    The original codes was written and provided by Silabs Corp
//    The codes was modified by changing some original codes and adding
additional codes by Dong D. Le
//-----------------------------------------------------------------------------
// Includes
//-----------------------------------------------------------------------------
#include <c8051f040.h>                // SFR declarations
#include <stdio.h>
#include <math.h>
#include <intrins.h>
#include <stdlib.h>
//-----------------------------------------------------------------------------
// 16-bit SFR Definitions for 'F04x
//-----------------------------------------------------------------------------
sfr16 DP       = 0x82;                // data pointer
sfr16 RCAP2    = 0xCA;                // Timer2 reload/capture value
sfr16 RCAP3    = 0xCA;                // Timer3 reload/capture value
sfr16 RCAP4    = 0xCA;                // Timer4 reload/capture value
sfr16 TMR2     = 0xCC;                // Timer2 counter/timer
```

```
sfr16 TMR3     = 0xCC;              // Timer3 counter/timer
sfr16 TMR4     = 0xCC;              // Timer4 counter/timer
sfr16 ADC0     = 0xBE;              // ADC0 data
sfr16 ADC0GT   = 0xC4;              // ADC0 greater than window
sfr16 ADC0LT   = 0xC6;              // ADC0 less than window
sfr16 DAC0     = 0xD2;              // DAC0 data
sfr16 DAC1     = 0xD2;              // DAC1 data
sfr16 CAN0DAT  = 0xD8;              // CAN data window
//-----------------------------------------------------------------------------
// Global Constants
//-----------------------------------------------------------------------------
#define BAUDRATE     115200          // Baud rate of UART in bps
#define SYSCLK       24500000        // Output of PLL derived from
(INTCLK*2)
#define INT_DEC      256             // Integrate and decimate ratio
#define SAR_CLK      2500000         // Desired SAR clock speed
#define SAMPLE_DELAY 30              // Delay in ms before displaying sample
#define ANALOG_INPUTS 4              // Number of AIN pins to measure
                                     // (min=1, max=8)
sbit LED = P1^6;                     // LED='1' means ON
sbit SW1 = P3^5;                     // SW1='0' means switch pressed
sbit SW2 = P3^6;
```

```
//-----------------------------------------------------------------------
// Function Prototypes
//-----------------------------------------------------------------------
void OSCILLATOR_Init (void);
void PORT_Init (void);
void UART1_Init (void);
void ADC0_Init (void);
void TIMER2_Init (void);
void TIMER4_Init (void);
void ADC0_ISR (void);
void TIMER2_ISR (void);
void Wait_MS (unsigned int ms);
//-----------------------------------------------------------------------
// Global Variables
//-----------------------------------------------------------------------
long Result[ANALOG_INPUTS];           // ADC0 decimated value, one for each
                                      // analog input
unsigned char amux_input=0;           // index of analog MUX inputs
unsigned char amux_convert=0;
//-----------------------------------------------------------------------
// main() Routine
//-----------------------------------------------------------------------
```

```
void main (void)
{
  int i, j, A;
  double count, Freq;
   long ME;

  WDTCN = 0xde;                    // Disable watchdog timer
  WDTCN = 0xad;
  OSCILLATOR_Init ();              // Initialize oscillator
  PORT_Init ();                    // Initialize crossbar and GPIO
  UART1_Init ();                   // Initialize UART1
  TIMER2_Init ();                  // Initialize Timer2 to overflow at 1 mS
  TIMER4_Init ();
  ADC0_Init ();                    // Init ADC
  SFRPAGE = ADC0_PAGE;
  AD0EN = 1;                       // Enable ADC
  EA = 1;                          // Enable global interrupts
  while (1)
  {
    EA = 0;                        // Disable interrupts
          SFRPAGE = CONFIG_PAGE;
    j = SW2;
```

```
        A = SW1;
count = 0;
        SFRPAGE = TMR4_PAGE;
TR4     = 1;                    // start Timer4
        TF4=0;                   // Set timer4 flag to 0


        while (TF4==0)
        {
         if (A != SW1)
                {
                 count = count+1;
                 A = SW1;
                }
}
          TR4 = 0;                              // Stop Timer4
        Freq = count;
         SFRPAGE = UART1_PAGE;
        printf("j=%d, Freq=%0.0lf,", j, Freq);
for(i=0; i<ANALOG_INPUTS; i++)
{
   // The 12-bit ADC value is averaged across INT_DEC measurements.
   // The result is then stored in Result, and is right-justified
```

```
      // The measured voltage applied to AIN 0.1 is then:
      //                      Vref (mV)
      //   measurement (mV) =   ---------- * Result (bits)
      //                    (2^12)-1 (bits)

      ME =  Result[i] * 2430 / 4095;
      printf(" AIN0.%d= %ld,",i,ME);
    }
      printf("\n");
    EA = 1;                     // Re-enable interrupts
    Wait_MS(SAMPLE_DELAY);          // Wait before displaying new values
  }
}
//-----------------------------------------------------------------------
// Initialization Subroutines
//-----------------------------------------------------------------------
//-----------------------------------------------------------------------
// SYSCLK_Init
//-----------------------------------------------------------------------
// Return Value : None
// Parameters   : None
// This routine initializes the system clock to use the internal oscillator
```

```
// at 24.5 MHz.
//-----------------------------------------------------------------------
void OSCILLATOR_Init (void)
{
  char SFRPAGE_SAVE = SFRPAGE;       // Save Current SFR page
  SFRPAGE = CONFIG_PAGE;             // set SFR page
  OSCICN = 0x83;                     // set internal oscillator to run
                                     // at its maximum frequency
  CLKSEL = 0x00;                     // Select the internal osc. as
                                     // the SYSCLK source
  SFRPAGE = SFRPAGE_SAVE;            // Restore SFR page
}
//-----------------------------------------------------------------------
// PORT_Init
//-----------------------------------------------------------------------
// Return Value : None
// Parameters   : None
// This routine configures the crossbar and GPIO ports.
//-----------------------------------------------------------------------
void PORT_Init (void)
{
  char SFRPAGE_SAVE = SFRPAGE;       // Save Current SFR page
```

```
  SFRPAGE = CONFIG_PAGE;            // set SFR page
  XBR0    = 0x00;
  XBR1    = 0x00;
  XBR2    = 0x44;                   // Enable crossbar and weak pull-up
                                    // Enable UART1
  P0MDOUT |= 0x01;                  // Set TX1 pin to push-pull
  P1MDOUT |= 0x40;                  // Set P1.6(LED) to push-pull
  SFRPAGE = SFRPAGE_SAVE;           // Restore SFR page
}
//-----------------------------------------------------------------------------
// UART1_Init
//-----------------------------------------------------------------------------
// Return Value : None
// Parameters   : None
//
// Configure the UART1 using Timer1, for <baudrate> and 8-N-1.
//-----------------------------------------------------------------------------
void UART1_Init (void)
{
  char SFRPAGE_SAVE = SFRPAGE;      // Save Current SFR page
  SFRPAGE = UART1_PAGE;
  SCON1   = 0x10;                   // SCON1: mode 0, 8-bit UART, enable RX
```

```
SFRPAGE = TIMER01_PAGE;
TMOD   &= ~0xF0;
TMOD   |=  0x20;                  // TMOD: timer 1, mode 2, 8-bit reload
if (SYSCLK/BAUDRATE/2/256 < 1) {
  TH1 = -(SYSCLK/BAUDRATE/2);
  CKCON |= 0x10;                  // T1M = 1; SCA1:0 = xx
} else if (SYSCLK/BAUDRATE/2/256 < 4) {
  TH1 = -(SYSCLK/BAUDRATE/2/4);
  CKCON &= ~0x13;                 // Clear all T1 related bits
  CKCON |=  0x01;                 // T1M = 0; SCA1:0 = 01
} else if (SYSCLK/BAUDRATE/2/256 < 12) {
  TH1 = -(SYSCLK/BAUDRATE/2/12);
  CKCON &= ~0x13;                 // T1M = 0; SCA1:0 = 00
} else {
  TH1 = -(SYSCLK/BAUDRATE/2/48);
  CKCON &= ~0x13;                 // Clear all T1 related bits
  CKCON |=  0x02;                 // T1M = 0; SCA1:0 = 10
}

TL1 = TH1;                        // initialize Timer1
TR1 = 1;                          // start Timer1
SFRPAGE = UART1_PAGE;
```

```
  TI1 = 1;                      // Indicate TX1 ready
  SFRPAGE = SFRPAGE_SAVE;       // Restore SFR page
}
//-----------------------------------------------------------------------
// ADC0_Init
//-----------------------------------------------------------------------
// Return Value : None
// Parameters   : None
// Configure ADC0 to use Timer2 overflows as conversion source, to
// generate an interrupt on conversion complete, and to use left-justified
// output mode.  Enables ADC end of conversion interrupt. Leaves ADC disabled.
//-----------------------------------------------------------------------
void ADC0_Init (void)
{
  char SFRPAGE_SAVE = SFRPAGE;       // Save Current SFR page

  SFRPAGE = ADC0_PAGE;
  ADC0CN = 0x0C;                // ADC0 disabled; normal tracking
                                // mode; ADC0 conversions are initiated
                                // on overflow of Timer2; ADC0 data is
                                // right-justified, low power tracking
                                // mode
```

```
  REF0CN = 0x03;                  // Enable on-chip VREF and output buffer
  AMX0CF = 0x00;                  // AIN inputs are single-ended (default)
  AMX0SL = 0x00;                  // Select AIN0.0 pin as ADC mux input
                                  // ISR will change this to step through
                                  // inputs
  ADC0CF = (SYSCLK/SAR_CLK) << 3;     // ADC conversion clock = 2.5MHz
  ADC0CF |= 0x00;                 // PGA gain = 1 (default)
  EIE2 |= 0x02;                   // enable ADC interrupts
  SFRPAGE = SFRPAGE_SAVE;         // Restore SFR page
}
//-----------------------------------------------------------------------------
// TIMER2_Init
//-----------------------------------------------------------------------------
// Return Value : None
// Parameters   : None
// Configure Timer2 to auto-reload at 20uS rate using SYSCLK as its timebase
//-----------------------------------------------------------------------------
void TIMER2_Init (void)
{
  char SFRPAGE_SAVE = SFRPAGE;       // Save Current SFR page
  SFRPAGE = TMR2_PAGE;
  TMR2CN = 0x00;                  // Stop Timer2; Clear TF2, select
```

```
                                // auto-reload;
  TMR2CF = 0x08;                // use SYSCLK as timebase, count down
  RCAP2   = 65536 -(SYSCLK / 24500);  // Init reload values for 20uS
  TMR2    = RCAP2;              // Set to reload immediately
  TR2     = 1;                  // start Timer2
  ET2     = 1;                  // enable timer 2 interrupt
  //IE |= 0x20;                 // enable timer 2 interrupt
  SFRPAGE = SFRPAGE_SAVE;       // Restore SFR page
}
//-----------------------------------------------------------------------------
// Interrupt Service Routines
//-----------------------------------------------------------------------------
//-----------------------------------------------------------------------------
// ADC0_ISR
//-----------------------------------------------------------------------------
// This ISR is called when the ADC0 completes a conversion.  Each value is
// added to a running total <accumulator>, and the local decimation counter
// <int_dec> decremented. When <int_dec> reaches zero, we post the decimated
// result in the global variable <Result[]>.
// The analog input is sampled, held, and converted on a Timer2 overflow.  To
// maximize input settling time, the analog mux is also advanced to the next
// input on the Timer2 overflow.  Two different indices are held globally:
```

```
//    amux_convert:  index of the analog input undergoing conversion
//    amux_input:    index of the analog input selected in the analog
//                   multiplexer
//-------------------------------------------------------------------------
void ADC0_ISR (void) interrupt 15
{
  static unsigned int_dec=INT_DEC;    // Integrate/decimate counter
                                      // we post a new result when
                                      // int_dec = 0
  static long accumulator[ANALOG_INPUTS] ={0L};
                                      // Here's where we integrate the
                                      // ADC samples from input AIN0.0
  int i;
  char SFRPAGE_SAVE = SFRPAGE;        // Save Current SFR page
  SFRPAGE = ADC0_PAGE;
  AD0INT = 0;                         //clear ADC conversion complete overflow
  accumulator[amux_convert] += ADC0;  // Read ADC value and add to running
                                      // total
  if(amux_convert == (ANALOG_INPUTS-1))// reset input index if the last input
                                      //was just read
    {
    int_dec--;                        // Update decimation counter
```

```
                        // when last of the analog inputs
                        // sampled
    }
  if (int_dec == 0)             // If zero, then post result
  {
    int_dec = INT_DEC;          // Reset counter
    for(i=0; i<ANALOG_INPUTS; i++)
      {
      Result[i] = accumulator[i] >> 8; //Copy decimated values into Result
      accumulator[i] = 0L;      // Reset accumulators
      }
  }
  amux_convert = amux_input;    // now that conversion results are
                        // stored, advance index to the analog
                        // input currently selected on the mux
  LED = 1;
  SFRPAGE = SFRPAGE_SAVE;       // Restore SFR page
}
//-----------------------------------------------------------------------------
// TIMER2_ISR
//-----------------------------------------------------------------------------
// The timer2 overflow triggers the ADC0 conversion on the analog MUX input
```

```
// previously selected.  It is permissable to change the analog MUX
// input once conversion has started, as the ADC has an internal sample
// and hold.
// This ISR routine will then select the next analog MUX input so as to
// maximize the settling time.
//-----------------------------------------------------------------------
void TIMER2_ISR(void) interrupt 5
{
  SFRPAGE = TMR2_PAGE;
  TF2 = 0;
  amux_input ++;                    // step to the next analog mux input
  if(amux_input == ANALOG_INPUTS)     // reset input index if the last input
    {                          // was just read
    amux_input=0;                 // reset input index back to AIN0.0
    }
  SFRPAGE = ADC0_PAGE;
  AMX0SL = amux_input;              // select the next input on the analog
                             // multiplexer
  LED = 0;
}
//-----------------------------------------------------------------------
// TIMER4_Init
```

```
//-----------------------------------------------------------------------
// Return Value : None
// Parameters   :
//   1)  int counts - calculated Timer overflow rate
//                  range is postive range of integer: 0 to 32767
// Configure Timer3 to auto-reload at interval specified by <counts> (no
// interrupt generated) using SYSCLK as its time base.
//-----------------------------------------------------------------------
void TIMER4_Init (void)
{
  char SFRPAGE_SAVE = SFRPAGE;        // Save Current SFR page
  SFRPAGE = TMR4_PAGE;
  TMR4CN = 0x00;                   // Stop Timer4; Clear TF4;
  TMR4CF = 0x00;                   // use SYSCLK as timebase
  RCAP4   = -(SYSCLK);              // Init reload values
  TMR4    = 0xfff;                 // Set to reload immediately
  EIE2   &= ~0x01;                 // Disable Timer3 interrupts
  TR4     = 1;                     // start Timer4
  SFRPAGE = SFRPAGE_SAVE;           // Restore SFR page
}
//-----------------------------------------------------------------------
// Support Subroutines
```

```
//-----------------------------------------------------------------------

//-----------------------------------------------------------------------

// wait_ms

//-----------------------------------------------------------------------

// This routine inserts a delay of <ms> milliseconds.

void Wait_MS(unsigned int ms)

{

  char SFRPAGE_SAVE = SFRPAGE;        // Save Current SFR page

  SFRPAGE = TMR3_PAGE;

  TMR3CN = 0x00;                      // Stop Timer3; Clear TF3;

  TMR3CF = 0x00;                      // use SYSCLK/12 as timebase

  RCAP3 = -(SYSCLK/1000/12);          // Timer 3 overflows at 1 kHz

  TMR3 = RCAP3;

  TR3 = 1;                            // Start Timer 3

  while(ms)

  {

    TF3 = 0;                          // Clear flag to initialize

    while(!TF3);                      // Wait until timer overflows

    ms--;                             // Decrement ms

  }


  TR3 = 0;                            // Stop Timer 3
```

```
  SFRPAGE = SFRPAGE_SAVE;          // Restore SFRPAGE
}
//-----------------------------------------------------------------------
// End Of File
//-----------------------------------------------------------------------
```

B5. PCB123 Circuit Board Layout Software [Ref 25]

"With the PCB123 V3 software you installed, you will be able to create a multi-page schematic by placing symbols that represent complete parts or sections of a part such as a gate, and then hooking them up with wires and special port symbols such as power and ground symbols.

Locating parts has never been easier. The part database is structured as a taxonomy which can be navigated in a tree or can be searched by typing in search criteria. Parts can contain a rich set of properties, all of which are searchable. This means you can search on a part by part number (Digikey or manufacturer) or by some characteristic such as ―4.99K, 1%‖.

Placing a part so its pins touch the pins of a different part will automatically generate wires between the pins as long as they are allowed by the rules. For instance, a power pin cannot be tied to a ground pin, and an NC pin (no connect) cannot be tied to anything. Wires can also be added by clicking on a pin or an existing wire (adding a junction) and then simply moving the mouse to the other pin/wire/junction and clicking again. This will automatically draw a wire that obeys the expected aesthetics. The auto-

wiring feature is invoked when an already-connected symbol is moved or rotated. Even high-pin-count symbols are neatly rewired as they are moved around. Even though auto-wiring is always in effect, you can also digitize corners exactly where you want them.

At any point you may flip over to the PCB view and you will see the new parts and their wires located at the system origin. You can select AutoPlace to rapidly position parts on the board. AutoPlace will attempt to minimize the overall interconnect distance between components while also locating the components in a reasonably aesthetic pattern. You can then examine and adjust the placement to perform local optimizations and enforce any special placement requirements that you may have.

At this point you may choose to autoroute the design. The autorouter will first escape surface mount pins to a via (a plated hole) to allow the router unrestricted access to all routing layers and or to connect to any internal plane layers. After fanout, the main autorouter will engage which attempts to add traces between objects that must be connected together. In many cases, the autorouter may not complete 100% of the connections or it may do so by using a topology that is unacceptable to you. In these cases, or in the event you just want to route the board completely by hand, there are very efficient editing tools to complete the task.

While manual routing or performing other PCB editing tasks by hand, a Design Rule Check (DRC) is performed in real-time and you will see DRC error markers come and go as you create and fix DRC violations. Whether autorouted or manually routed, you can at any stage choose to run the Gloss command to remove redundant corners, segments, and vias.

You not only have the ability to designate internal plane layers, but you can also choose to view them as positive or negative images. In addition, you may wish to fill in unoccupied areas on the routing layers of the board with copper planes. These planes are typically assigned to a net such as GND and will connect to any pins inside the plane region that are tied to the same net. It does so not with a direct hit between the plane and the pin, but through thermal reliefs to aid soldering.

Nomenclature may be added to the board as copper or on silkscreen layers using text strings or drawn polygonal features.

A full DRC (Design Rule Check) can be run on the board when it is believed to be complete. A full DRC will check for violations of net rules such as adherence to minimum spacing requirements, shorts, and opens. It will also check for possible manufacturing problems such as drill excursions into SMD features, silkscreen in holes or on SMD features, and even isolated pins in copper pour regions.

It is recommended that a final visual check of the PCB be done with the 3D viewer. The photorealistic rendering system displays the board in a perspective projection and allows the board to be viewed from any angle in 3D space. It is good for identifying problems that the DRC engine might otherwise deem valid. These may include problems with drill sizes, holes where there should be none, missing holes, plated/unplated hole problems, and unreadable silkscreens.

At any time, either the schematic or the layout may undergo component or net additions, deletions, or changes and the other will be synchronized. This makes tasks

such as adjusting the number of decoupling capacitors based on available real estate or routing density a snap.

Finally, when the design is complete you can press the Order button to begin the process of getting your circuit boards manufactured".

REFERENCES LIST

1. D.D.L. Chung, “Composites get smart”, Materials Today, pp: 30-35, January 2002.
2. D.D.L. Chung, “Piezoresistive cement-based materials for strain sensing”, Journal of Intelligent Material Systems and Structures, vol. 00, pp: 1-12, December 2002.
3. D.D.L. Chung, “Composite Materials: Science and Applications”, London, Springer, 2003.
4. X. Wang and D.D.L. Chung, “Self-monitoring of fatigue damage and dynamic strain in carbon fiber polymer-matrix composite”, Composites: Part B, 29B (1):63-73, 1998.
5. J.P. Lynch, A. Sundararajan, K.H. Law, H. Sohn and C.R. Farrar, “Design of a wireless active sensing unit for structural health monitoring”, *SPIE 11th Annual International Symposium on Smart Structures and Materials*, San Diego, CA, USA, March 14-18, 2004.
6. X. Wang and D.D.L. Chung, “Real-time monitoring of fatigue damage and dynamic strain in carbon fiber polymer-matrix composite by electrical resistance measurement”, Smart Mater. Struct., 6:504-508, 1996.
7. W.J. McCarter, O. Vennesland, “Sensor systems for use in reinforced concrete structures”, Construction and Building Materials 18 (2004) 351-358.
8. P.A.M. Basheer, P.R.V. Gilleece, A.E. Long and W.J. McCarter,”Monitoring electrical resistance of concretes containing alternative cementitious materials to

assess their resistance to chloride penetration", Cement and Concrete Composites 24 (2002), 437-449.

9. T.L. Floyd, "Electric Circuits Fundamentals", third edition. New Jersey: Prentice Hall, 1995.
10. L. J. Van der Pauw, "Determination of resistivity tensor and hall anisotropic conductors," *Philips Res. Rept.*, vol. 16, pp. 187-195, 1961.
11. S. Putta, V. Vaidyanathan and J. Chung, "Development and testing of a nodal resistance measurement (NRM) system for composite structures", Measurement 41 (2008) 763-773.
12. X. Fu, E. Ma, D.D.L Chung and W.A. Anderson, "Self-monitoring in carbon fiber reinforced mortar by reactance measurement", Cem. Concr. Res., 28(2); 183-187, 1997.
13. S. Mingquing, L. Qingping, L. Zhuoqiu and H. Yaozu, Cem. "A study of piezoelectric properties of carbon fiber reinforced concrete and plain cement paste during dynamic loading", Concr. Res., 30(10):1593-1595, 2000.
14. S. Vidhate, J. Chung, V. Vaidyanathan and N. D'Souza, Time dependent piezoresistive behavior of polyvinylidine fluoride/carbon nanotube conductive composite, Materials Letters (In press, 2009).
15. M. Lentner, and T. Bishop, "Experimental Design and Analysis", second edition, Virginia: Valley Book Company, 1993.

16. R. Prabhakaran, “Damage assessment through electrical resistance measurement in graphite fiber-reinforced composites”. 9th International Conference on Experimental Mechanics, Copenhagen, Denmark, August, 1990.
17. S. Wang, and D.D.L. Chung, “Self-sensing of flexural strain and damage in carbon fiber polymer-matrix composite by electrical resistance measurement”. Carbon Volume 44, Issue 13, November 2006, 2739-2751.
18. D.D.L. Chung and S. Wang, “Self-sensing of damage and strain in carbon fiber polymer-matrix structural composites by electrical resistance measurement”, J. Polymers and Polymer Composites,Vol. 11(7), p. 515-525, 2003.
19. National Semiconductor. "LM1575/LM2575/LM2575HV-Simple Switcher® 1A Step-Down Voltage Regulator." *National.com.* 04 2007. http://www.national.com/ds/LM/LM1575.pdf (accessed 2009).
20. Silicon Laboratories. "C8051F04X Development Kit User’s Guide." *Silabs.com.* 09 06. https://www.silabs.com/Support%20Documents/TechnicalDocs/C8051F04x-DK.pdf (accessed 09).
21. Silicon Laboratories. "C8051F040/1/2/3/4/5/6/7." *Silabs.com.* Rev. 1.5. https://www.silabs.com/Support%20Documents/TechnicalDocs/C8051F04x.pdf (accessed 2009).
22. EXAR. "XR-2206 Monolithic Function Generator." *Exar.com.* 02 2008. http://www.exar.com/Files/Documents/XR2206_104_020808.pdf (accessed 2009).

23. Analog Devices. "AD636 - Low Level, True RMS-to-DC Converter." *Analog.com.* 2006. http://www.analog.com/static/imported-files/data_sheets/AD636.pdf (accessed 2009).
24. Keil. *C51 Development Tools.* 2009. http://www.keil.com/c51/ (accessed 2009).
25. Sunstone Circuits. "PCB123 Version 3: User Guide and Reference manual." *Sunstone.com.* 2007. http://www.sunstone.com/downloads/v3%20guide.pdf (accessed 2009).
26. Silicon Laboratories. “Over View”, CD Development Kit Tool & Documentation. Release 2.82©2006.
27. National Semiconductor. "LM117/LM317A/LM317-3 Terminal Adjustable Regulator." *National.com.* 10 20, 2008. http://www.national.com/ds/LM/LM117.pdf (accessed 2009).
28. Shoukai Wang, D.D.L. Chung and Jaycee H. Chung, “Self-sensing of damage in carbon fiber polymer matrix composite by measurement of the electrical resistance or potential away from the damage region,” Journal of Material Science, 40, pp 6463-6472, October 2005.
29. Daojun Wang, Shoukai Wang, D.D.L. Chung and Jaycee H. Chung, “Sensitivity of the two-dimensional electrical potential/resistance method for damage monitoring in carbon fiber polymer-matrix composite,” Journal of Material Science, 41, pp. 4839-4846, May, 2006.

30. Daojun Wang, Shoukai Wang, D.D.L. Chung and Jaycee H. Chung, "Method of Sensing Impact Damage in Carbon Fiber Polymer-Matrix Composite by Electrical Resistance Measurement", J. Mater. Sci. 41(8), 2281-2289 (2006).
31. Jaycee Chung and D.D.L. Chung, *Composite Self-Diagnosis via Electrical Resistance Measurement*, AFOSR F49620-03-C-0087 STTR Final Report, June 2004.
32. L. Shen, J. Li, B.M. Liaw, F. Delale and J.H. Chung, "Modeling and Analysis of the Electrical Resistance Measurement of Carbon Fiber Polymer-Matrix Composites," *Composite Science and Technology*, Vol. 67, Issues 11-12, pp. 2513-2520, 2007.
33. Y. Ngabonziza, H. Ergun, R. Kuznetsova, B.M. Liaw, J. Li, F. Delale and J.H. Chung, "A Feasibility Study of Self-Diagnosis of Interlaminar Damage in Carbon-Fiber Composites," accepted for publication in *Journal of Intelligent Material Systems and Structures* (Special Issue on SI-SMASIS-SHM, Manuscript No.: JIMSS-09-008).
34. Y. Ngabonziza, H. Ergun, R. Kuznetsova, J. Li, B.M. Liaw and F. Delale, "Structural Self-Diagnosis for Damage in Carbon-Fiber Reinforced Composites," Proceedings of the ASME Conference on Smart Materials, Adaptive Structures and Intelligent Systems", Ellicott City, MD, October 28-30, 2008, Paper No. SMASIS2008-365.
35. E. Sevkat, J. Li, B.M. Liaw, F. Delale, and J.H. Chung, Electrical Resistance Method for Self-Sensing of Damage in Carbon Fiber-Reinforced Composites, *Macro- to Nano-scale Inelastic Behavior of Materials: Plasticity, Fatigue, and Fracture*, ed. by A.S. Khan and B. Farrokh, Neat Inc. Press, 2009, pp. 247-249.

36. Y. Ngabonziza, C. Boldrini, B.M. Liaw, J. Li, F. Delale and J.H. Chung, “Fatigue Damage Self-Sensing of Composites via Electrical Resistance Measurements,” presented in the Symposium on Self-Sensing, Self-Healing, Self-Powering and Multifunctional Materials at the 3rd International Conference on Integrity, Reliability & Failure (IRF’2009), Porto, Portugal, July 20-24, 2009.
37. Yves Ngabonziza, Hale Ergun, Regina Kuznetsova, Jackie, Li, Ben Liaw, Feridun Delale and Jaycee Chung, “An Experimental Study of Self-Diagnosis of Interlaminar Damage in Carbon Fiber Composites,” J. of Intelligent Material Systems and Structures, accepted for publication, Manuscript ID: JIMSS-09-008.R2, 2009.